Cell Biology
Neuroscience

Endosomal sorting protein SNX4 limits synaptic vesicle docking and release

Reviewed Preprint
v2 • November 26, 2024
Revised by authors

Reviewed Preprint
v1 • May 7, 2024

Josse Poppinga, Nolan J Barret, L Niels Cornelisse, Matthijs Verhage, Jan RT van Weering

Department of Functional Genomics, Center for Neurogenomics and Cognitive Research (CNCR), VU University, Amsterdam, The Netherlands • Department of Human Genetics, CNCR, Amsterdam UMC, Amsterdam, The Netherlands

https://en.wikipedia.org/wiki/Open_access
Copyright information

eLife Assessment

This **important** study presents a series of results aimed at uncovering the involvement of the endosomal sorting protein SNX4 in neurotransmitter release. While the evidence supporting the conclusions is **solid**, the molecular mechanisms remain unclear. This paper will be of interest to cell biologists and neurobiologists.

https://doi.org/10.7554/eLife.97910.2.sa4

Abstract

Sorting nexin 4 (SNX4) is an evolutionary conserved organizer of membrane recycling. In neurons, SNX4 accumulates in synapses, but how SNX4 affects synapse function remains unknown. We generated a conditional SNX4 knock-out mouse model and report that SNX4 cKO synapses show enhanced neurotransmission during train stimulation, while the first evoked EPSC was normal. SNX4 depletion did not affect vesicle recycling, basic autophagic flux or the levels and localization of SNARE-protein VAMP2/synaptobrevin-2. However, SNX4 depletion affected synapse ultrastructure: an increase in docked synaptic vesicles at the active zone, while the overall vesicle number was normal, and a decreased active zone length. These effects together lead to a substantially increased density of docked vesicles per release site. In conclusion, SNX4 is a negative regulator of synaptic vesicle docking and release. These findings suggest a role for SNX4 in synaptic vesicle recruitment at the active zone.

Endosome sorting plays a critical role in the recycling and degradation of proteins in various eukaryotic cell types, including neurons (Cullen & Steinberg, 2018; Huotari & Helenius, 2011; Sardana & Emr, 2021; Vietri et al., 2020). Synapses, in particular, rely on rapid recycling mechanisms to replenish synaptic vesicles (SVs) and facilitate neurotransmitter release (Kononenko & Haucke, 2015; Rizzoli, 2014; Südhof, 2000). The extent to which endosome sorting is involved in these processes has been a subject of ongoing debate since the early studies on SV recycling (Ceccarelli et al., 1973; Heuser & Reese, 1973; Kononenko & Haucke, 2015; Watanabe & Boucrot, 2017). While it has been demonstrated that depleting endosomal proteins

affect neurotransmitter release (Chen et al., 2017; Tagliatti et al., 2016; Uytterhoeven et al., 2011), the precise role of these sorting proteins on SV maintenance and fusogenity remains not well understood.

Sorting nexins (SNXs) are evolutionary conserved organizers of endosome sorting that are recruited to endosome membrane domains by a phox homology (PX) domain (Carlton et al., 2005). SNX4 belongs to a subgroup of SNXs containing a C-terminal a Bin–Amphiphysin– Rvs (BAR) domain that recognizes and remodels curved endosome membranes (Cullen & Steinberg, 2018; Teasdale et al., 2001; Van Weering et al., 2012). While several SNX-BARs are associated with the retromer-related Endosomal SNX-BAR Sorting Complex for Promoting Exit (ESCPE)-1 (Simonetti et al., 2023), SNX4 forms a distinct sorting complex with SNX7, SNX30 (Antón et al., 2020; van Weering et al., 2012), SNX5 (Zhou et al., 2022), or SNX32 (Sugatha et al., 2023) for endosome-to-cell surface recycling pathways and autophagosome traffic (Traer et al., 2007; Van Weering et al., 2012; Zhou et al., 2022). SNX4 emerges as a central hub in this endosome recycling pathway as the expression of SNX4 is required for the stable SNX7 and SNX30 protein levels in cells (Antón et al., 2020). SNX4 is expressed in all cell types but to what extent this conserved principle also operates in highly polarized mammalian cells, such as neurons, remains unclear. In post-mortem brain material of Alzheimer's disease patients, altered protein levels of SNX4 have been observed (Kim et al., 2017). SNX4 is implicated in the recycling of the amyloid precursor protein cleaving enzyme (BACE-1), sorting it away from the endolysosomal pathway (Kim et al., 2017; Toh et al., 2018). Consequently, dysregulation of SNX4 may lead to the mislocalization of BACE-1 to late endosomal compartments, potentially contributing to altered amyloid-ß-production. In yeast, Snx4 is essential for the endosome recycling of Snc1p, a homolog of the SNARE protein VAMP2/synaptobrevin-2 (VAMP2/syb2) that is essential for synaptic transmission (Hettema et al., 2003; Ma et al., 2017; Schoch et al., 2001). In neurons, SNX4 specifically accumulates in synapses, and its knockdown dysregulates protein pathways involved in neurotransmission (Vazquez-Sanchez et al., 2020). While its synaptic subcellular localization has been shown, the functional role of SNX4-dependent endosome sorting in synapses remains unknown.

In this study, we characterize the role of endosomal sorting protein SNX4 in synapse function using a novel conditional SNX4 knock-out mouse model. We show that SNX4 limits synaptic vesicle docking and release. SNX4 depletion enhances neurotransmission specifically during train stimulation, while the first evoked response is not significantly affected. SNX4 depletion does not impact vesicle recycling or the levels and localization of the SNARE-protein VAMP2/syb-2. The overall number synaptic vesicles is unaffected in SNX4 cKO neurons, but these synapses show an increased number of docked synaptic vesicles at the active zone of the presynapse. The active zone length is decreased, thereby further increasing the density of synaptic vesicles at the release site of SNX4 cKO synapses. Our data collectively shows that the endosomal sorting protein SNX4 is a negative regulator of synaptic vesicle docking and release.

Results

Neuronal SNX4 protein levels are depleted in 21 days in conditional SNX4 knock out mouse primary cultures

We generated a conditional knock-out mouse model for SNX4 (**Fig. 1a** and materials and methods section) to circumvent previously reported off-target effects using shRNA approaches (Vazquez-Sanchez et al., 2020). In neuronal cultures, SNX4 has a half lifetime of 10.6 days (Dörrbaum et al., 2018). To test SNX4 optimal knock out efficiency, cKO neurons were fixed after 21 days *in vitro* (DIV21) and Cre expression was initiated at different time points (DIV7, DIV3, and DIV0) (**Fig. 1b**). SNX4 expression was detected by western blot which showed a reduction of 67% after 14 days of cre, 83% after 18 days of cre and 90% after 21 days of cre compared to control

neurons infected with delta-Cre (**Fig. 1c, d**). Immunohistochemistry of SNX4 in primary hippocampal neurons showed a 64% reduction in SNX4 in MAP2-neurites after 21 days of expressing cre (**Fig. 1e, f**). Morphological parameters such as dendrite length and dendrite branching, based on MAP2 staining, and synapse number, based on VAMP2 puncta, remained unaffected in SNX4 cKO neurons (**Fig. 1 f-i** & **Fig. 4a**). These data show a successful depletion of 90% of endosomal sorting protein SNX4 using a novel conditional knock-out mouse model for SNX4.

SNX4 depletion enhances neurotransmission during train stimulation

To investigate the functional role of SNX4 in synapses, we studied the effect of SNX4 depletion on neurotransmission by electrophysiological recordings in single hippocampal neurons cultured on glia micro-islands (autapse) at DIV21 (**Fig. 2a**). Both the amplitude and charge of the first evoked response showed a non-significant trend towards an increase in SNX4 cKO neurons (KO) compared to neurons infected with delta-Cre (control) (**Fig. 2b, c** & d). The rescue condition where SNX4 was re-expressed at DIV14 (KO + SNX4) showed a decreased amplitude compared to KO but not to control. A similar trend was observed for total charge (**Fig. 2b, d**). Paired pulse ratios were not affected in SNX4 cKO neurons (**Fig. 2e**). We next investigated the effect of SNX4 depletion on synaptic transmission during sustained activity using a series of train stimulations at 5, 10 and 40Hz (results in **Supplementary table 1**, **Supplementary Fig S2**). During a train of 100 action potentials at 40 Hz, the charge in SNX4 cKO neurons was highly increased (**Fig. 2f, h**). The average charge between pulse 90-100 was increased by 110% in SNX4 cKO synapses compared to control (**Fig. 2g**). SNX4 overexpression rescued this increase in charge to WT levels (**Fig. 2f, g** &h). The size and refilling of the readily releasable vesicle pool (RRP) was estimated using back extrapolation of the cumulative charge (**Fig. 2h**) (Schneggenburger et al., 1999). While we found no significant differences in RRP estimate size in SNX4 cKO synapses compared to control (**Fig. 2i**), the slope estimate of the cumulative charge was increased upon SNX4 depletion, which was rescued by SNX4 overexpression (**Fig. 2j**). The amplitude and frequency of spontaneous miniature EPSCs (mEPSCs) were not affected upon SNX4 depletion (**Fig. 2k-m**). In order to investigate a direct effect of SNX4 overexpression on neurotransmission, we expressed exogenous SNX4 on wild-type control background. Both the amplitude and charge of the first evoked response showed no effect in control + SNX4 neurons compared to control, and no differences were detected in the response to the 40 Hz stimulation train (**Supplementary Fig. 3a-e**), indicating that SNX4 overexpression in itself does not affect the neurotransmission protocols studied in SNX4 cKO experiments. Together these data show enhanced neurotransmission during train stimulation in SNX4 cKO autapses, while single EPSCs, mEPSCs and the RRP size estimate remain unaffected. This suggests that vesicle recruitment during high frequency train stimulation is limited by SNX4.

Synaptic vesicle recycling and retrieval are not altered in SNX4 cKO neurons

As the recruitment rate of releasable vesicles during train stimulation was increased in SNX4 cKO neurons, we assessed its role in synaptic vesicle recycling using the synaptic vesicle fusion reporter synaptophysin-super-ecliptic-pHluorin (SypHy) (Granseth et al., 2006). Neurons were stimulated by two trains of 100 action potentials at 40 Hz. The total pool of SypHy in acidified SVs per synapse was determined by NH4 superfusion (**Fig. 3a, b**). SNX4 cKO neurons showed a higher fluorescence intensity upon both stimulation trains (**Fig. 3c**), represented as the stimulated fraction (**Fig. 3d, e**), and return to baseline fluorescence level within 60 seconds over a total imaging time course of 160 seconds (**Fig. 3c**). The fluorescence decay time constant tau in the 60 s after electrical stimulation, a measure for SV endocytosis, was not changed after both stimuli in SNX4 cKO neurons (**Fig. 3f**). Finally, the responding fluorescent puncta during action

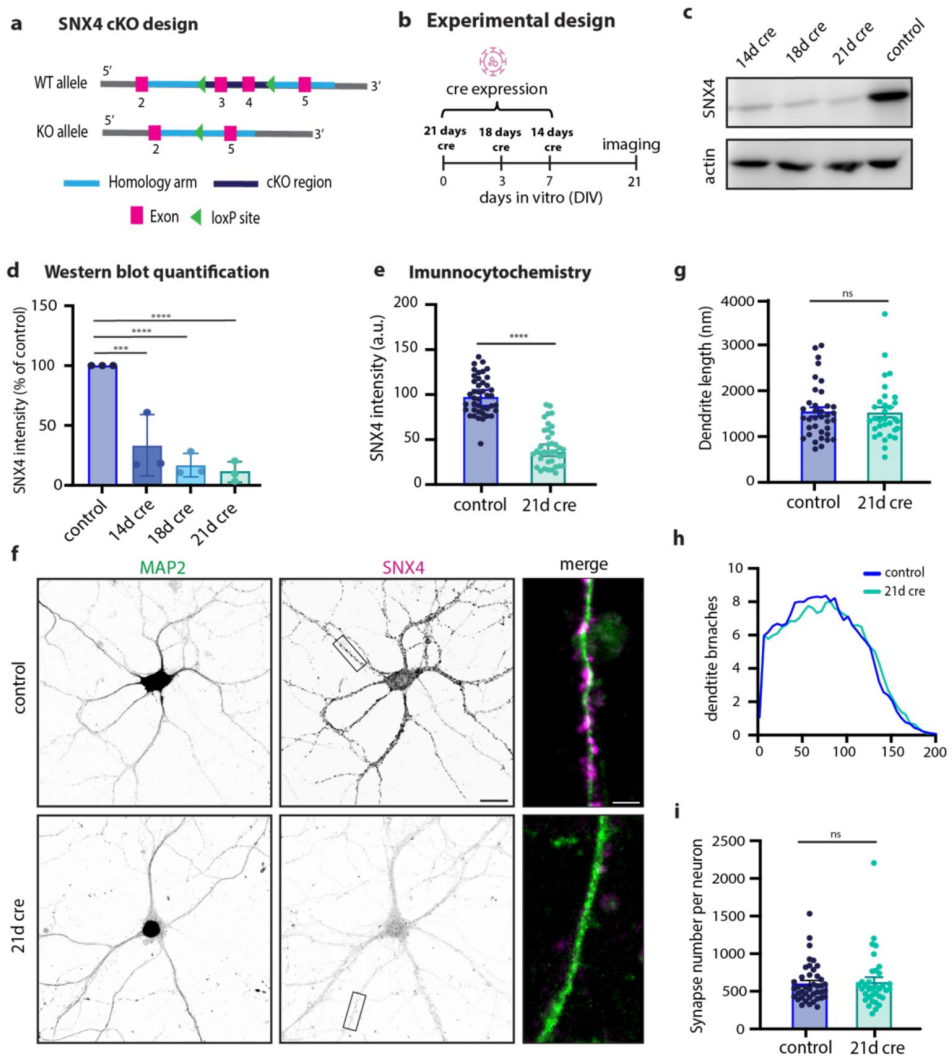

Figure 1

SNX4 is knocked-out in primary hippocampal neurons using a novel conditional knock-out mouse line.

(a) Schematic overview of conditional knock-out design of SNX4. **(b)** Schematic overview of experimental design using cre intervention at different DIVs. **(c)** Typical example of western blot of SNX4 and actin at 14 days, 18 days and 21 days of cre and control (delta cre) expression. **(d)** Quantification of western blot SNX4 protein levels for control (dcre), 14 days of cre, 18 days of cre and 21 days of cre, normalized to control. **(e)** Quantification of immunocytochemistry SNX4 intensity normalized to control. **(f)** Typical example of primary hippocampal neurons stained for SNX4 (magenta) and map2 (green) for control and 21 days of cre. Scale bar = 20 µm. Zoom-in scale bar = 3 µm. **(g)** Dendrite length for control and KO hippocampal neurons. **(h)** Sholl analysis for number dendrite branches. **(i)** Number of synapses per neuron (MAP2 mask) based on VAMP2 puncta (shown in **Fig. 4**) ****p=<0.0001, ***p=0.0003, **p=0.0005, *p=0.0019. Ordinary one-way ANOVA with Tukey's multiple comparisons test for **(d)** with N=3 animals. Mann-Whitney test for **(e)** with n=32-42 neurons per group and N=6 animals and. Data points represent individual western blots/neurons; bar graph represents mean with SEM.

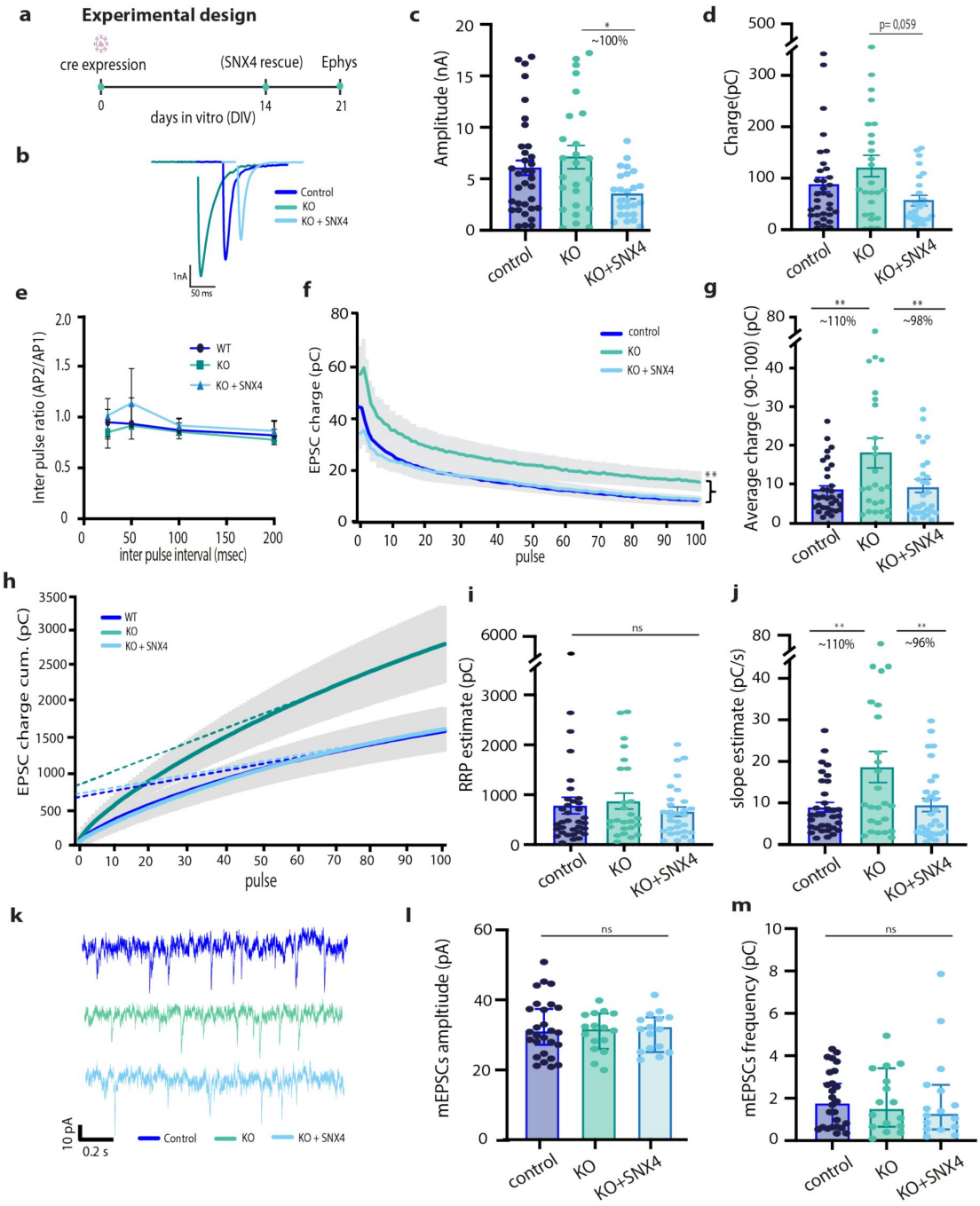

Figure 2

SNX4 depletion increases sustained synaptic vesicle release.

(a) Schematic overview of experimental design using cre intervention at DIV0, SNX4 rescue at DIV14 and recording at DIV21. **(b)** Representative traces of the first evoked response for control, KO and KO+SNX4 upon stimulation. **(c)** Amplitude of first evoked response. **(d)** Charge of first evoked response. **(e)** Paired pulse ratios of amplitude at inter pulse intervals of 25, 50, 100 and 200 msec. **(f)** Mean EPSC charge trace for 100 AP at 40 Hz train. **(g)** Average charge at pulse 90-100. **(h)** Cumulative EPSC charge for 100 AP at 40 Hz train with back extrapolation linear fit to AP 80-100. **(i)** Estimate of RRP based on back extrapolation (h). **(j)** Estimate of slope based on based on back extrapolation **(k)** representative traces of mEPSC response for control, KO and KO+SNX4 **(l)** mEPSC amplitude (**m)** mEPSC frequency. Multilevel ANOVA with n = 25-38 neurons per group of N = 3-4 animals. ***p < 0.0001, **p < 0.001. Data points represent individual neurons; bar graph represents mean with SEM.

potential stimulation as a ratio of the total fluorescent puncta during NH4, the percentage of active synapses, showed a trend towards fewer active synapses in SNX4 cKO neurons (**Fig. 3g**). Hence, these data show that SNX4 depletion enhances synaptic vesicle release without altering synaptic vesicle recycling and the number of active synapses in hippocampal neurons.

It has, however, been shown that different SV recycling pathways dominate at different temperatures (Watanabe et al., 2013). To test if SNX4 affects SV recycling at physiological temperatures, we used a FM4-64 dye loading protocol before electrical field stimulation (**Fig. 3h**). Recycling SVs were labelled by a 60s-incubation with FM4-64 in 60mM K^+ at 37^0C. Vesicle fusion was triggered by a train of action potentials at 40 Hz, resulting in a decreased FM4-64 fluorescence intensity (**Fig. 3h, i**). SNX4 cKO neurons showed a similar fluorescence intensity decay after electrical stimulation over a total imaging time course of 80 seconds (**Fig. 3j**). The average fluorescence signal in the last 10 seconds normalized to baseline (F/F0), a measure for the total amount of recycling synaptic vesicles fusing, was not significantly different between control and SNX4 cKO neurons (**Fig. 3k**). FM4-64 uptake, a measure for endocytosis at 37 ^{0}C, was also not altered in SNX4 cKO neurons (**Fig. 3l**). Taken together, these data suggest that SNX4 depletion does not affect synaptic vesicle endocytosis and recycling both at room temperature and physiological temperature.

SNX4 depletion does not affect synaptic VAMP2/syb-2 levels and distribution or autophagy markers in neurons

In yeast, it is reported that SNX4 homologue Snx4p mediates retrieval of Snc1p, yeast's VAMP2/syb-2 homologue (Hettema et al., 2003; Ma et al., 2017). Missorting of VAMP2 in neurons could affect synaptic transmission. Therefore, we investigated VAMP2/syb-2 as potential cargo of SNX4. To test whether SNX4 mediates VAMP2/syb-2 retrieval in neurons, we investigated the localization, number and expression levels of VAMP2/syb-2 upon SNX4 knock-out by immunohistochemistry. SNX4 immunostaining showed clear co-localization with VAMP2/syb-2 (**Fig. 4a**). In SNX4 cKO neurons, no significant difference was found in VAMP2/syb-2 puncta number per µm dendrite or VAMP2/syb-2 intensity (**Fig. 4a, b, c**). Sholl-analysis of average VAMP2/syb-2 intensity over distance from soma also revealed no differences in VAMP2/syb-2 localization upon SNX4 depletion (**Fig. 4d**). Western blot analysis revealed no changes in total VAMP2/syb-2 protein levels (**Fig. 4e**). These data show that SNX4 is not required for a normal VAMP2/syb-2 distribution and protein level, as observed for the yeast orthologs of both proteins. Other potential cargos of SNX4 that could affect neurotransmission include those involved in the autophagy pathway (Antón et al., 2020; Kuijpers et al., 2021). We investigated autophagy markers and autophagosomes following SNX4 depletion, using P62 as a basal autophagic receptor marker and bafilomycin to inhibit autolysosome formation, thereby assessing basal autophagic flux. In SNX4 cKO neurons, there was no significant difference in P62 puncta numbers or P62 somatic intensity under basal conditions or after bafilomycin treatment, suggesting that autophagic flux remains normal (**Supplementary Fig. 4a, b, c**). Western blot analysis also showed no changes in total ATG5 protein levels (**Supplementary Fig. 4d&e**) and ultrastructural analysis revealed no differences in the total number of autophagosomes (**Supplementary Fig. 4f&g**). Collectively, these data indicate that SNX4 depletion does not impact the basal autophagic flux, ATG5 protein levels, or the number of autophagosomes.

Presynaptic ultrastructure and synaptic vesicle docking are affected in SNX4 cKO synapses

Next, we sought to further investigate synapse organization upon SNX4 depletion using electron microscopy (**Fig 5a**). The number of docked vesicles was measured by direct contact of vesicles with the active zone plasma membrane (**Fig. 5a,b**). The average synaptic vesicle size, defined by all clear core vesicles smaller than 50 nm, was reduced by 5%, whereas vesicles larger than 50 nm,

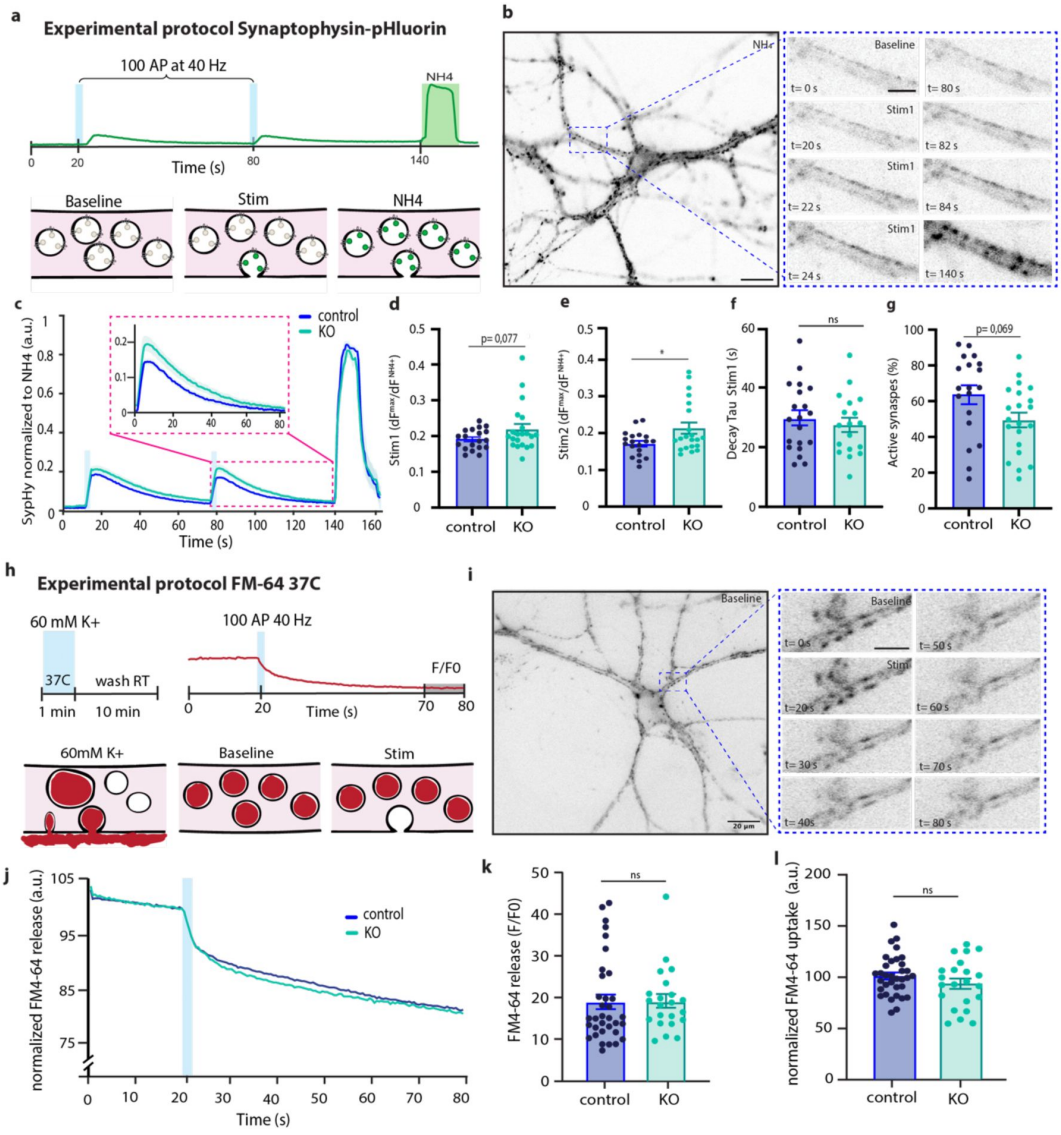

Figure 3

SNX4 depletion does not affect synaptic vesicle recycling at room temperature and physiological temperatures.

(a) Stimulation paradigm with a single vesicle fluorescence intensity trace**. (b, Left)** Representative image of a SypHy–infected neuron during Tyrode's NH4 application (Scale bar: 20 µm.). **(Right)** Neurite before (baseline) and during (100 AP at 40 Hz) stimulation and during NH4 application (NH4) (Scale bar: 10 µm.). **(c)** The average fluorescence normalized from baseline to maximum SypHy intensity during Tyrode's NH4 application. **(d)** Maximum response amplitude during the first electrical stimulation normalized to maximum NH4 response plotted as $\Delta F^{max}/F^{NH4}$**. (e)** Maximum response amplitude during the second electrical stimulation normalized to maximum NH4 response plotted as $\Delta F^{max}/F^{NH4}$**. (f)** Fluorescence decay time constant tau in the 60 s after electrical stimulation representing SV endocytosis and acidification **(g)** Percentage active synapses. **(h)** Stimulation paradigm with a single vesicle fluorescence intensity trace. Recycling SVs are labelled by 60s-incubation with FM4-64 in 60mM K+ at 37C, followed by a 10min washout. Electrical field stimulation (100AP, 40Hz) triggers SV exocytosis recorded as decreased FM4-64 fluorescence intensity. **(i, Left)** Representative image of FM64-dye endocytosed by a neuron during baseline (Scale bar: 20 µm.). **(Right)** Neurite before (baseline) and during (100 AP at 40 Hz) stimulation (Scale bar: 10 µm.). **(j)** The average FM4-64 fluorescence traces, normalized to control baseline, over time showing initial SV loading, followed by release after electrical field stimulation. **(k)** FM4-64 release upon electrical field stimulation **(l)** FM4-64 uptake (upon 60 mm K^+ incubation). Multilevel ANOVA with N=3 animals and n=21-24 neurons per group for SypHy experiment and N=4 animals with n=28-36 neurons per group for FM64-dye experiment. Bar graph represents mean with SEM. Data points represent individual fields of view.

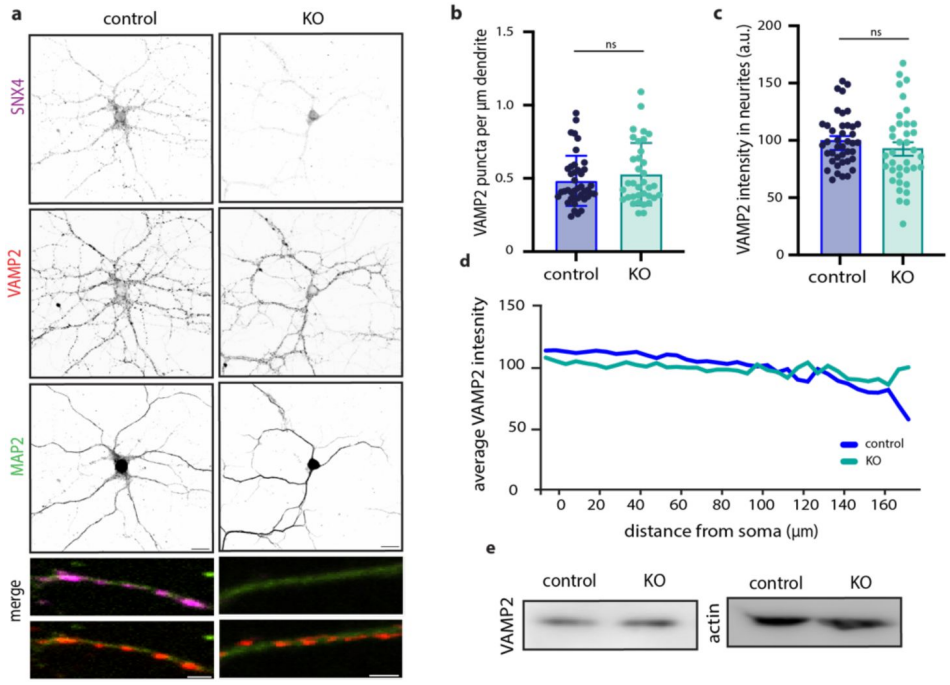

Figure 4

SNX4 depletion does not decrease VAMP2 levels and localization.

(a) Typical example immunocytochemistry images of primary hippocampal neurons stained for SNX4 (magenta), VAMP2 (red) and MAP2 (green) from control and SNX4 cKO mice. Scale bar = 20 µm. Merge zoom-in scale bar = 2 µm. **(b)** VAMP2 puncta per µm dendrite for control and KO. **(c)** VAMP2 intensity measured in dendrites. **(d)** Sholl analysis of average VAMP2 intensity over distance from the soma for control and KO. **I** Western blot of SNX4, VAMP2, and actin for control and KO. Data points represent individual neurons, N=6 animals and n=35-41 neurons for VAMP2 data, bar graphs represent mean with SEM.

did not show significant changes upon SNX4 depletion (**Fig. 5c, d**). Additionally, the distribution of vesicles, grouped by bin size of 10 nm, showed no notable differences upon SNX4 depletion. (**Supplementary Fig. 5**). In SNX4 cKO synapses, the number of docked vesicles was significantly higher than in control (**Fig. 5a, f**) whilst the total number of vesicles was not altered (**Fig. 5e**). When normalized to the active zone length, the density of docked vesicles at the active zone length further increases by 50% in SNX4 cKO synapses compared to control (**Fig. 5g**). Moreover, we observed a significant decrease in active zone length, PSD length and vesicle cluster area (**Fig. 5g-j**). Together these data show that SNX4 depletion affects the presynaptic ultrastructure, characterized by smaller active zone length and vesicle cluster area, suggesting a decrease in overall synapse size. In these smaller synapses, SNX4 cKO neurons contain more docked synaptic vesicles leading to a substantially increased density of docked vesicles per release site.

Discussion

In this study we addressed the role of SNX4-dependent endosome sorting in synapses, using a new conditional SNX4 knock-out mouse model. We show that SNX4 cKO synapses elicit enhanced neurotransmission during train stimulation. SNX4 depletion did not affect vesicle recycling, basal autophagic flux or the levels and localization of SNARE-protein VAMP2/syb-2. Electron microscopy showed that synapses had an increased number of docked vesicles at the active zone, while the overall number of synaptic vesicles was normal. The active zone length was decreased upon SNX4 depletion, thereby further increasing the density of docked synaptic vesicles at the release site. Taken together, our data shows that the endosomal sorting protein SNX4 is a negative regulator of synaptic vesicle docking and release. These findings indicate that SNX4 regulates synaptic vesicle recruitment at the active zone.

Enhanced SV recruitment and increased SV docking explain increased transmission in SNX4 cKO synapses

SNX4 cKO synapses showed a 110% increase in neurotransmission during intense stimulation (**Fig. 2f**). A trend towards increased neurotransmission was observed already from the start of the train, and also in single evoked responses (**Fig. 2c-d**), but became more prominent (and significant) during sustained stimulation. Despite the variability within all datasets, both trends and the significant effect during sustained stimulation were fully reversed by acute SNX4 expression. The total number of synapses (**Fig 1h**) and fraction of active synapses (**Fig 3g**) was not affected in SNX4 cKO neurons, suggesting an intrasynaptic effect. While approximately twice more vesicles were released during sustained stimulation in the absence of SNX4 (**Fig. 2f**), our RRP estimation indicated a normal resting state RRP (**Fig. 2i**). All measures of release probability were normal (normal paired pulse facilitation, **Fig. 2e**, and shape of the rundown curve, **Fig. 2f**), indicating that an increased release probability is an unlikely explanation for the observed increase in neurotransmission during sustained stimulation. The mEPSC recordings were also not affected (**Fig. 2k-m**), this is consistent with the unaffected RRP estimate and single EPSC size and suggests that the observed increase in neurotransmission is not due to post-synaptic effects.

Hence, this suggests that a higher recruitment rate of SVs to the releasable pool (**Fig. 2h, j**) in SNX4 cKO synapses is responsible for the increased neurotransmission. While back extrapolation methods for estimating the RRP have their limitations (Neher, 2015) and mechanisms of SV recruitment remain not fully understood, it is evident that the involvement of newly recruited vesicles becomes more prominent during high frequency trains. In line with this, the increased neurotransmission of SNX4 cKO neurons was less prominent in 5Hz and 10Hz trains (Fig S2). Hence, an increased contribution of newly recruited vesicles during sustained stimulation is consistent with the fact that neurotransmission is increased especially during high frequency

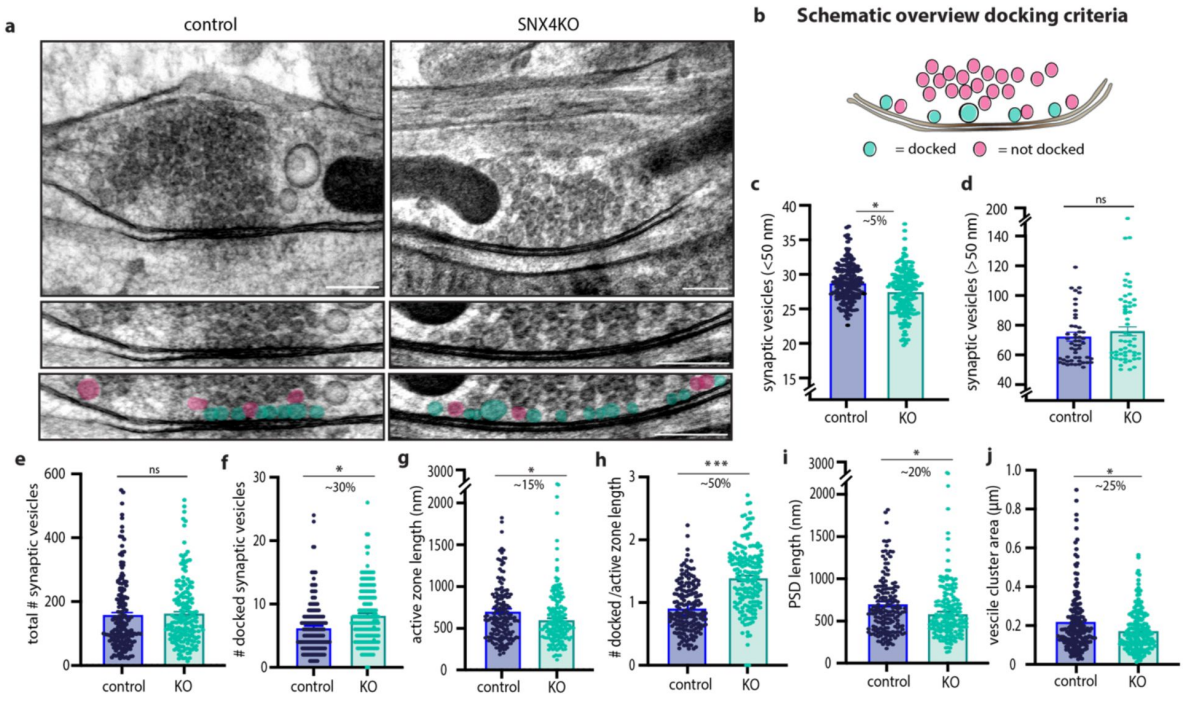

Figure 5

SNX4 depletion increases the number of docked vesicles at the active zone.

(a) Example micrographs of control and SNX4 cKO synapses (Scale bar: 200 nm) with zoom in on the active zone region indicating docked (blue) and non-docked vesicles (pink) (Scale bar : 100 nm) **(b)** Schematic overview of docked and undocked vesicles. **(c & d)** The average vesicle size, distinguished between synaptic vesicles (<50 nm) and larger clear core vesicles (>50 nm). **(e)** The total amount of synaptic vesicles in the synaptic cloud. **(f)** The number of docked synaptic vesicles in control and SNX4 cKO synapses**. (g)** The active zone length. **(h)** The number of docked vesicles normalized to active zone length**. (i)** The post synaptic density (PSD) length. **(j)** The area of the vesicle cloud in control and SNX4 cKO synapses. Bar graphs represent mean with SEM with n = 174-175 synapses per group of N = 3 animals. Data points are individual synapses. ***p < 0.0001, **p < 0.001 using Mann-Whitney test.

stimulation in SNX4 cKO synapses. No effects on neurotransmission were observed when overexpressing SNX4 on a control background, indicating that SNX4 is required but not rate limiting to limit synaptic release during prolonged stimulation.

The increase in neurotransmission during sustained stimulation was also observed with synaptic vesicle fusion reporter SypHy but not with the FM-64 dye. The latter method reports the release of only recycled vesicles, suggesting that these do not contribute significantly to the enhanced release. Finally, examining SV recycling with FM-64 dye indicates that the increased SV recruitment in SNX4 cKO synapses is not driven by an enhanced rate of the synaptic vesicle cycle, as endocytosis and release of recycled SVs were normal in SNX4 cKO synapses.

Ultrastructural characterization of SNX4 cKO synapses revealed a 50% increase in docked vesicles when normalized to active zone length. This increase might contribute to the enhanced SV recruitment and increased neurotransmission observed in SNX4 cKO synapses. If more vesicles are already docked at the start of stimulation, they may on average be recruited faster during train stimulation. Synaptic vesicle docking is probably a dynamic equilibrium between various synaptic vesicle pools, modulated by activity (Kusick et al., 2020). However, an increase in docked SVs at the active zone also implies, on average, a closer proximity to calcium channels and therefore a higher release probability. However, measures of release probability were unaffected by SNX4 deficiency (as argued above) suggesting a normal channel coupling in SNX4 cKO synapses.

SNX4 at the crossroad of endosomal sorting and autophagy regulating synaptic output

Increased neurotransmission upon depletion of endosomal genes has been shown by several labs (Fernandes et al., 2014; Soykan et al., 2021; Tagliatti et al., 2016; Uytterhoeven et al., 2011). These results are consistent with a postulated hypothesis that endosomes act sorting stations for SV proteins and control the balance between novel and reused SV proteins that affect SV release and neurotransmission efficiency (Fernandes et al., 2014; Truckenbrodt et al., 2018; Uytterhoeven et al., 2011).

In the presence of SNX4, the recycling process may lead to the re-use of older SV proteins that, as indirect consequence, potentially diminish the efficiency of SV exocytosis. In the absence of SNX4, older SV proteins are less recycled and traffic towards degradation, rendering the synapse with relatively more novel SV proteins, enhancing SV recruitment and fusion. Blocking the degradation pathway with HOPS/ESCRT mutants rescues the observed increased release(Fernandes et al., 2014; Uytterhoeven et al., 2011). Similarly, Skywalker and ARF6 mutants show increased SV sorting through endosomal intermediates, increasing SV docking and release (Fernandes et al., 2014; Tagliatti et al., 2016; Uytterhoeven et al., 2011). Our data is consistent with this literature, demonstrating enhanced neurotransmission upon inactivation of an endosome sorting gene. That said, SNX4 cKO synapses do not show an accumulation of endosomal intermediates (**Fig 5d**) or decreased SV numbers (**Fig 5e**) as reported for other endosome gene mutants, marking a novel finding in endosomal protein knockout studies.

Endosomal sorting also mediates the delivery of active zone proteins, where disturbances in these pathways potentially correlate with smaller active zones and SVs, ultrastructural phenotypes we also observed in SNX4 cKO synapses. Previous studies suggest that the removal of SNX4 directs its cargo toward the degradative pathway (Hettema et al., 2003; Traer et al., 2007). Although the SNX4 cargo, particularly in mammalian neurons, is currently unknown, it is unlikely that VAMP2/syb-2 recycling explains our phenotype since the overall levels and localization of VAMP2/syb-2 remained unaffected upon SNX4 depletion.

Apart from endosome sorting, SNX4 has been reported to regulate several types of autophagy (Antón et al., 2020; Hanley et al., 2021; Zhou et al., 2022). Recent literature has shown that synaptic vesicle release could be regulated by synaptic autophagy (reviewed by Decet & Verstreken, 2021). Loss of ATG5 has been shown to result in increased neurotransmission, an effect independent from total SVs pool number (Kuijpers et al., 2021). We did not observe changes in total ATG5 levels upon SNX4 depletion, consistent with previous reports, (Antón et al., 2020), and no difference in basic autophagic flux of P62, contrasting with previous findings in HeLa cells (Antón et al., 2020). This suggests that SNX4 may have a specialized role in neurons, that regulates synaptic transmission independent of autophagic flux by a yet-to-be determined mechanism.

SNX-BAR proteins critical for synapse function

Many of our examined synaptic parameters remained unaltered or showed considerable variability, including our hypothesis that depletion of a synaptic endosomal sorting protein would disrupt synaptic recycling. This suggests the presence of redundant pathways compensating for SNX4 depletion, potentially involving other SNX-BAR complexes or endosomal sorting complexes like ESCPE, retriever, or retromer (Simonetti et al., 2023). Particularly SNX-BAR proteins, such as SNX7 and SNX30, are of potential interest for future research due to their ability to form selective complexes with SNX4 (Antón et al., 2020). The role of endosome sorting in the synaptic vesicle cycle is increasingly recognized through knockout studies targeting various endosomal complexes, revealing changes in SV exocytosis, SV endocytosis, or endosome-like vesicle numbers (X. Chen et al., 2017; X. W. Chen et al., 2008; Inoshita et al., 2017; Tagliatti et al., 2016). Our data supports this, showing for the first time that a protein from the highly evolutionary conserved SNX-BAR protein family, such as SNX4, regulates SV docking at the active zone and sustained SV release. Taken together, we show that endosomal sorting protein SNX4 regulates synaptic vesicles recruitment at the active zone. The precise regulation of vesicle availability is crucial for a synapse to effectively coordinate neurotransmission, a process heavily relying on endosome sorting mechanisms.

Materials and methods

Laboratory animals and SNX4 cKO generation

Animals were housed and bred according to institutional and Dutch governmental guidelines (DEC-FGA 11-03 and AVD112002017824). The SNX4 conditional KO targeting strategy aimed to achieve mouse SNX4 gene loss of function by flanking exon 3 and 4 with loxP sites to acutely remove these exons by Cre recombinase (**Fig 1a**). In the targeting vector, self-deletion anchor sites flank the Neomycin cassette, and Diphtheria toxin A fragment (DTA) is used for negative selection. Mouse genomic fragments containing homology arms were amplified from a BAC clone using high-fidelity Taq DNA polymerase. These fragments were then sequentially assembled into a targeting vector along with the recombination sites and selection markers. Homologously targeted $SNX4^{lox}$ embryonic stem cells (C57BL/6) were injected into blastocysts and implanted into pseudopregnant females to produce germ-line chimeras, which were mated with inbred C57BL/6 mice. The mouse colony was maintained by homozygous lox/lox mice breeding, with every third or fourth generation mice were backcrossed with C57BL/6 mice. The following primers were used for genotyping: forward primer: TTCTTGAGGGTAACAGAAATCCTTAGTGCC and reverse primer CTCTGAATACCAGGAGAGTCCACAAGAGC.

Primary neuronal cultures

Dissociated hippocampal neuron cultures were prepared from P01 SNX4KO mouse embryos. Hippocampi dissected free of meninges in Hanks' balanced salt solution (Sigma, H9394) supplemented with 10 mM HEPES (Gibco, 15630-056). The hippocampi were isolated from the

tissue and digested with 0.25% trypsin (Gibco, 15090-046) in Hanks' HEPES for 20 min at 37°C. Hippocampi were washed three times with Hanks' HEPES and triturated with fire-polished glass pipettes. Neurons were counted and plated in Neurobasal medium (Gibco, 21103-049) supplemented with 2% B-27 (Gibco, 17504-044), 1.8% HEPES, 0.25% Glutamax (Gibco, 35050-038), and 0.1% penicillin–streptomycin (Gibco, 15140-122). Hippocampal neurons were plated in 12-well plates at a density of 25.000 cells per well on 18-mm glass coverslips containing rat glia or 50.000 cells on coverslips containing 0.01% Poly-ornithin (Sigma P4957) and 2.5 ug/ml laminin coating (Sigma L2020) solution o/n at RT. Neuronal cultures were kept in supplemented Neurobasal at 37°C and 5% CO2 until DIV21.

Constructs and lentiviral infection

Neuronal cultures were infected with EGFP-Cre and EGFP-control (delta Cre) at DIV0 to generate SNX4KO. All constructs were cloned into lentiviral vectors under the synapsin promoter, and lentiviral particles were generated following the protocol previously described in (Naldini et al., 1996).The presence of an EGFP nuclear localization sequence (NLS) allowed identification of tranduced cells (Kaeser et al., 2011). For synaptic vesicle release experiments, neurons were infected with Synaptophysin-pHluorin lentivirus at DIV7. Titration of lentiviral particle batches was performed by assessment of number of fluorescent cells upon infection to ensure 100% infection efficiency. For rescue experiments and SNX4 overexpression experiments a lentiviral construct of mouse SNX4 was generated with an ECFP fluorescent tag together with an 2A cleavage site in between in a FUW backbone (pECFP-T2A-SNX4(mus musculus)- FUW).

Western blot

Cortical neurons at DIV21 were washed with phosphate-buffered saline (PBS) and lysed in Laemmli sample buffer consisting of 2% SDS (VWR chemicals, M107), 10% glycerol (Merck, 818709), 0.26 M b-mercaptoethanol (Sigma, M3148), 60 mM Tris-HCl (Serva, 37180) pH 6.8, and 0.01% Bromophenol blue (Applichem, A3640). Samples of 450.000 neurons run in SDS-PAGE (10% 1 mm acrylamide gel with 2, 2, 2-Trichloroethanol) using standard SDS-PAGE technique and transferred into polyvinylideenfluoride membranes (Bio-rad) (1 hour, 0.25 mA, 4 C°). Blots were blocked and incubated with primary antibodies (4 degrees O/N) in PBS containing 0.1% Tween-20 (Sigma, P2287) (PBS-T) and 5% milk. Primary antibodies included polyclonal rabbit SNX4 (1:500; SySy, Cat. No. 392 003), monoclonal mouse actin (1:10000; Chemicon, Cat. No. MAB1501), monoclonal mouse VAMP2/synaptobrevin2 (1:2000; SySy, CL 69.1), and polyclonal rabbit BACE-1 (1:500; Abcam ab20770). After washing with PBS-T, blots were incubated with secondary horseradish peroxidase (HRP)-labeled antibodies (1:10000; Sigma) in PBS-T and 5% milk (1 hour, RT). After washing with PBS-T, blots were developed with SuperSignal West Femto substrate (Thermo Scientific, 11859290) for 2 min. Chemiluminescence labelled proteins were visualised with the Odyssey Imaging System (LI-COR) for appropriate times and analysed with Image Studio 5.2 software (LI-COR) or ImageJ. A fixed region of interest (ROI) was used to measure the average intensity, which was then normalized to 1) the loading control (housekeeping genes Actin or GAPDH) and 2) the control within each independent experiment (N) to account for weekly variations.

Immunocytochemistry

Neurons at DIV21 were fixed in 3.7% formaldehyde (Electron Microscopies Sciences, 15680) in PBS, pH 7.4, for 25 min at RT. After washing with PBS, cells were permeabilized for 5 min with 0.5% Triton X-100 (Fisher Chemical, T/3751/08)–PBS and incubated for 30 min with PBS containing 2% normal goat serum (Gibco, 16210-072) and 0.1% Triton X-100 to block nonspecific binding. Incubations with primary antibodies were performed O/N at 4°C. After PBS washing steps incubations with secondary antibodies followed for 1h at RT. Primary antibodies included polyclonal rabbit SNX4 (1:500; SySy, Cat. No. 392 003), monoclonal mouse VAMP2/synaptobrevin2 (1:1000; SySy, CL 69.1), and polyclonal chicken MAP2 (1:300; Abcam ab5392) and Alexa Fluor

conjugated secondary antibodies (1:1000; Invitrogen). Coverslips were mounted with Dabco-Mowiol 4-88 (Sigma, 81381) and confocal microscope (Nikon eclipse Ti) using a 40× oil immersion objective (NA = 1.3)) was used to examine the samples. Laser settings were kept constant within experimental conditions.

Electrophysiological recordings

Autaptic cultures of *SNX4* null neurons were grown for 21–25 days before measuring. Whole-cell voltage-clamp recordings (*V*m = −70 mV) were performed at room temperature with borosilicate glass pipettes (2.5–4.5 mOhm) filled with 136 mM KCl, 17.8 mM HEPES, 0.6 mM MgCl2, 4 mM ATP-Mg, 0.3 mM GTP-Na, 12 mM phosphocreatine dipotassium salt, 45.3 mM phosphocreatine kinase, and 1 mM EGTA (pH 7.30). External solution contained the following (in mM): 10 HEPES, 10 glucose, 140 NaCl, 2.4 KCl, 4 MgCl2, and 4 CaCl2 (pH = 7.30, 300 mOsmol). Recording was acquired with an MultiClamp 700B amplifier (Molecular Devices), Digidata 1550B, and Clampex 9.0 software (Molecular Devices). After whole-cell mode was established, only cells with an access resistance of < 15 MΩ and leak current of < 300 pA were accepted for analysis. Serie resistance compensation was between 70-80%. Access resistance was measured before and after recordings. Recordings with a > 20% increase in access resistance were excluded from analysis, as well as recordings that showed voltage clamp escape or clipping. GABAergic recordings were identified based on their postsynaptic decay kinetics and excluded. EPSCs were elicited by a 1-ms depolarization to 30 mV. Offline analysis was performed with MATLAB R2019a (Mathworks) using custom-written software routines (viewEPSC, downloaded from user vhuson on Github on 13 Sept 2023). RRP and slope estimates were obtained by a linear fit of cumulative total charge plot from pulse 80 to 100 for each individual cell with y-intercept for RRP estimate and slope as recruitment rate estimate (Schneggenburger et al., 1999).

Live cell imaging

Live imaging experiments were performed at DIV21 on a custom build imaging microscope (IX81; Olympus) with an MT20 light source (Olympus) with a 40× oil objective (NA=1.3) appropriate filter sets (semrock, Rochester, NY) and an EM charge-coupled device camera (C9100-02; Hamamatsu Photonics, Japan). Xcellence RT imaging software (Olympus) controlled the microscope and image acquisition. Coverslips were perfused with Tyrode's solution (119 mM NaCl, 2.5 mM KCl, 2 mM $CaCl2^{-}$ 2H2O, 2mM $MgCl2^{-}$ 6H2O, 25 mM HEPES, and 30 mM glucoseH2O, pH 7.4, mOsmol 280). For synaptic vesicle release experiments, time-lapse (2 Hz) recordings consisted of 30 s baseline recordings followed by two electrical field stimulations with 60s recovery time in between and a final stimulation 10s of NH4-Tyrode's perfusion (2 mM CaCl2, 2.5 mM KCl, 119 mM NaCl, 2 mM MgCl2, 30 mM glucose, 25 mM HEPES, 50 mN NH4Cl at pH 7.4). Electrical field stimulation was applied via parallel platinum electrodes powered by a stimulus isolator (WPI A385) delivering 30-mA, 1-ms pulses, regulated by a Master-8 pulse generator (A.M.P.I.) providing 100 APs at 40 Hz with a 0.5-s interval. Glass capillaries close to the isolated neuron were used for chemical stimulation. For the FM4-64 experiments, neurons were pre imaging incubated in high potassium Tyrode's for 10 min at 37 C°(61.5 mM NaCl, 60 mM KCl, 2 mM CaCl22H2O, 2mM MgCl2 6H2O, 25 mM HEPES and 30 mM glucoseH2O, pH 7.4, mOsmol 280).

Imaging analysis

For live-cell imaging analysis, timelapse recordings stacks were used to analyze SyPhy and FM4-64 fusion events (2 Hz, 1000 × 1000pixels). In ImageJ fusion events were selected manually and fluorescence traces were measured in a circular 3 × 3 pixel ROI (0.6 x 0.6 um), somatic events not included. ROI intensity measures of SyPhy puncta were exported to a custom-built Matlab program for semiautomated detection of fusion events and duration (Moro et al., 2021). Fluorescence traces from the ROI were expressed as fluorescence change (deltaF) compared to initial fluorescence (F0), with the average of frames 1-10 for determining F0. Fusion events were automatically detected when displaying a sudden increase of two standard deviations above F0.

Synaptic vesicle pool numbers and synapses were estimated using MAP2 mask in automated image analysis software SynD (Schmitz et al., 2011). Active synapses were determined by 3x SD over baseline. Synapse detection settings were optimized to measure SyPhy and VAMP2/syb-2 puncta signal and kept constant within the same dataset. For FM4-64 puncta, fluorescence traces were expressed as change (DF) compared to baseline fluorescence (F0) and the average of the last 10 frames was used to determine the maximum FM4-64 release.

For fixed cell imaging analysis, VAMP2 puncta number within MAP2 mask were analysed using automated SynD software (see above). For sholl analysis, dendrite mask based on MAP2 staining was used to either determine the number of dendritic branches per shell or average VAMP2 intensity within the neurite mask.

Cryofixation electron microscopy

Dissociated hippocampal neurons (5000 k/well) from SNX4 cKO mice were plated on pre-grown cultures of rat glia on sapphire disks (Wohlwend GmbH) to form micro-networks of 2– 10 neurons per sapphire disk. Prior to cell culture, sapphire disks were etched for 30 minutes in 60% sulfuric acid, washed, incubated in 3M KOH overnight, washed and dried before carbon coating and subsequent baking at 180 C for 2 hours. Sapphire discs were coated by a mixture of 0.1 mg/ml poly-d-lysine (Sigma), 0.7 mg/ml rat tail collagen (BD Biosciences), and 10 mM acetic acid (Sigma) and placed in an agarose-coated 12-well plate to form glia monolayer islands selectively on sapphire disks. The sapphire disks were cryofixed in an EM-PACT2 (Leica Microsystems) high-pressure freezer in 5% trehalose/10% BSA in 0.05M phosphate buffer pH 7.4 320 mOsm cryoprotectant. Frozen samples were postfixed in 1% OsO4/ 5% saturated K4Fe(CN)6 in H2O in acetone at −90°C for 74 hours and brought to 0°C at 5°/h. After a couple washes with ice-cold acetone, the sapphire disks were washed with propylene oxide and with an increasing Epon concentration series. The samples were embedded in fresh Epon overnight and left to polymerize at 65°C for 48 h. Sapphire disks were separated from the Epon by dipping the samples in boiling water and liquid nitrogen and regions with micro-networks were selected by light microscopy. These regions were cut out and mounted on pre-polymerized Epon blocks for ultrathin sectioning. Ultrathin sections (80 nm) were cut parallel to the sapphire disk, collected on single-slot, formvar-coated copper grids, and stained in uranyl acetate and lead citrate. Hippocampal synapses were randomly selected at low magnification using an electron microscope (JEOL1010), and the conditions were blinded. For each condition, the number of docked SVs, total SV number, and active zone length were measured on digital images taken at 80,000-fold magnification using custom-written semiautomatic image analysis software running in Matlab (Mathworks). For all morphological analyses the following requirements were set: clearly recognizable synapses with intact synaptic plasma membranes with a recognizable pre- and postsynaptic area and defined SV membranes. SVs were defined as docked if there was no distance visible between the SV membrane and the active zone membrane (pixel size 0.6505 nm).

Statistics

Data are shown as mean +- SEM. Data that violated both normality (Shapiro-Wilk) and homogeneity (Levene test) was tested with the two-sided Mann–Whitney U test. Data exhibiting a normal distribution yet significantly altered variation were tested with Welch's t-test. When assumptions of homogeneity and normality were met, data were tested with Student's t test or one-way ANOVA with Tukey's multiple comparisons test. For the analysis of electron microscopy data, electrophysiology data and live cell imaging (pHluorin and FM dye), the intraclass correlation coefficient (ICC) was calculated for different variables applicable to each experiment such as culture batch, sapphire or synapse originating from the same neuron. If ICC was close to 0.1 or above, indicating that a considerable portion of the total variance can be attributed to e.g. culture week, multilevel analysis was performed to accommodate nested data (Aarts et al.,

2014). For electrophysiology data, we excluded outliers beyond mean ± 3xSD. Bar graphs were plotted as the mean with SEM, where individual data points represent fields of view, neurons or synapses (EM data set).

Acknowledgements

The authors thank dr. Sander Groffen for help with the conditional knock-out mouse design, Joke Wortel for housing and breeding the mice, Desiree Schut for helping with neuronal cultures, Robbert Zalm for cloning and lentiviral production, Marien P Dekker for assistance with EM analysis. We thank Jill Gerritsen for electrophysiology data analysis. We would like to thank Elise van Bree and Sonia Vazquez-Sanchez for their pioneering work on synaptic release in SNX4 shRNA models. The van Weering lab is supported by Alzheimer Nederland (WE.03-2019-06).

Author contributions

J.P. performed experiments and analyzed the data. N.J.B. and L.N.C collected and analyzed Ephys data. J.R.T.vW collected and analyzed EM data. J.P., M.V. and J.R.T.vW designed the experiments and wrote the manuscript with input of all authors.

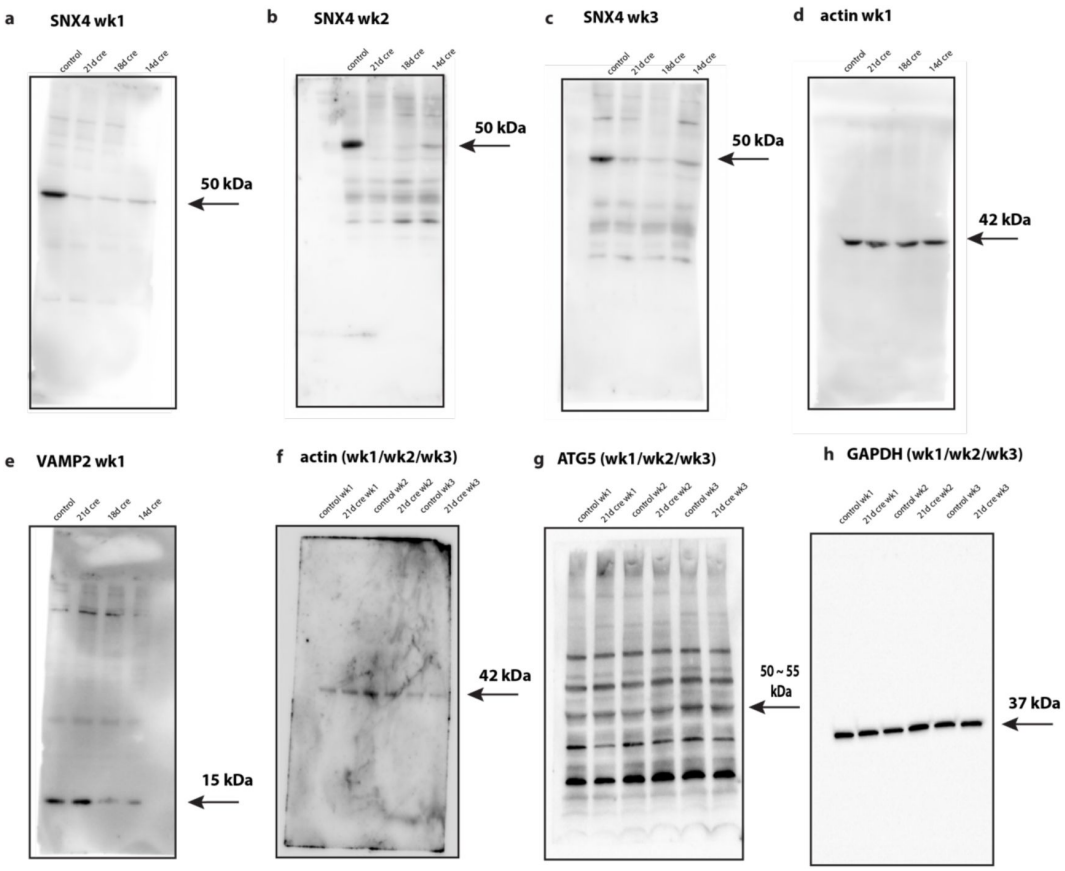

Supplementary figure 1

Overview of uncropped blots used for western blot analysis. (a,b,c)

SNX4 at 50 kDa for control (21 days of dcre), 21 days of cre, 18 days of cre and 14 days of cre. Repeated for three different animals, wk1 is normalized to actin and wk2 and wk3 are normalized to unspecific band on the blot. Fold of change is determined for all weeks by normalizing to control per week. **(d)** Actin at 42 kDa for control, 21 days of cre, 18 days of cre and 14 days of cre. Same animal and transfer as SNX4 wk1. **(e)** VAMP2 at 15 kDa for control, 21 days of cre, 18 days of cre and 14 days of cre. Same animal and transfer as SNX4 wk1. **(f)** Actin at 42 kDa for control and 21 days of cre for three different animals on one blot. (**g)** ATG5 at 55bkDa for control and 21 days of cre for three different animals on one blot. (**h)** GAPDH at 42 kDa for control and 21 days of cre for three different animals on one blot.

Supplementary figure 2

EPSC charge for 5 Hz and 10 Hz train stimulation.

(a) Mean EPSC charge trace for 100 AP at 5 Hz train. **(b)** Mean EPSC charge trace for 100 AP at 10 Hz train.

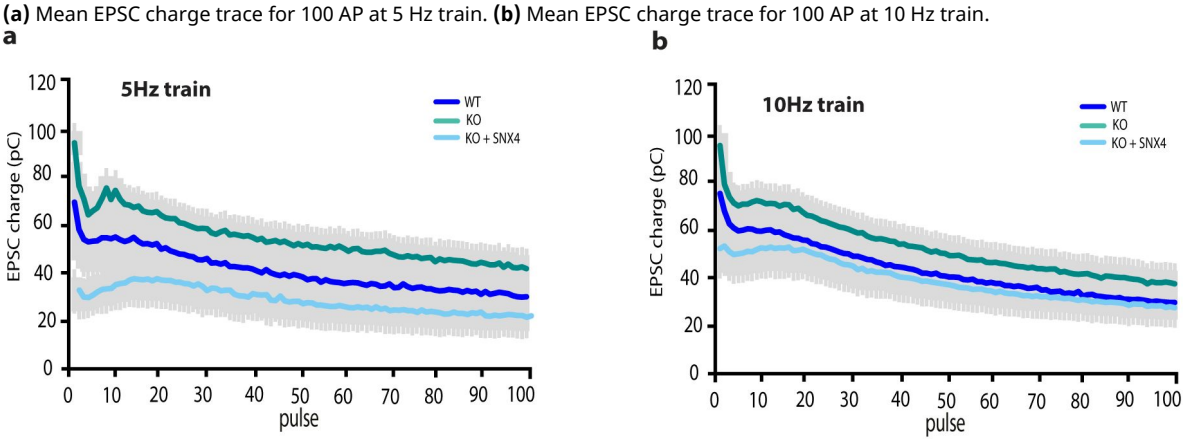

Supplementary 3

SNX4 overexpression does not affect first evoked EPSC or neurotransmission during sustained release.

(a) Representative traces of the first evoked response for control and control+SNX4 upon stimulation. **(b)** Amplitude of first evoked response. **(c)** Charge of first evoked response. **(d)** Mean EPSC charge trace for 100 AP at 40 Hz train. **(e)** Average charge at pulse 90-100. Multilevel ANOVA with n = 22-26 neurons per group of N = 4-6 animals. Data points represent individual neurons; bar graph represents median + 95% confidence interval.

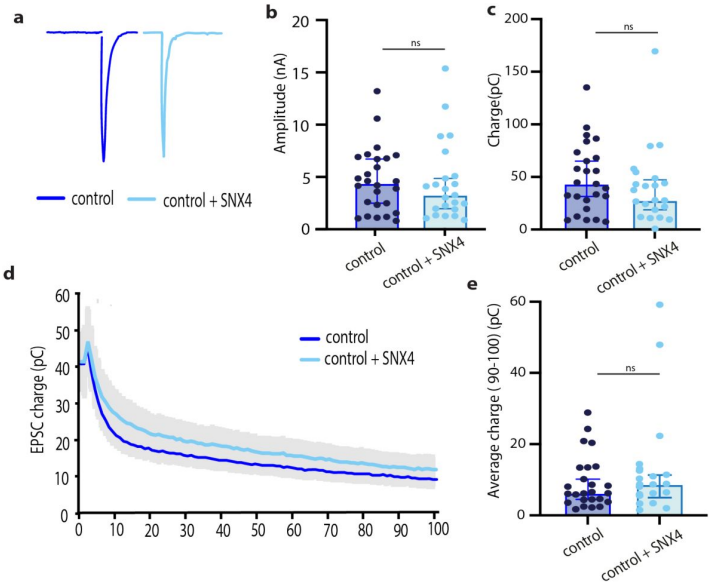

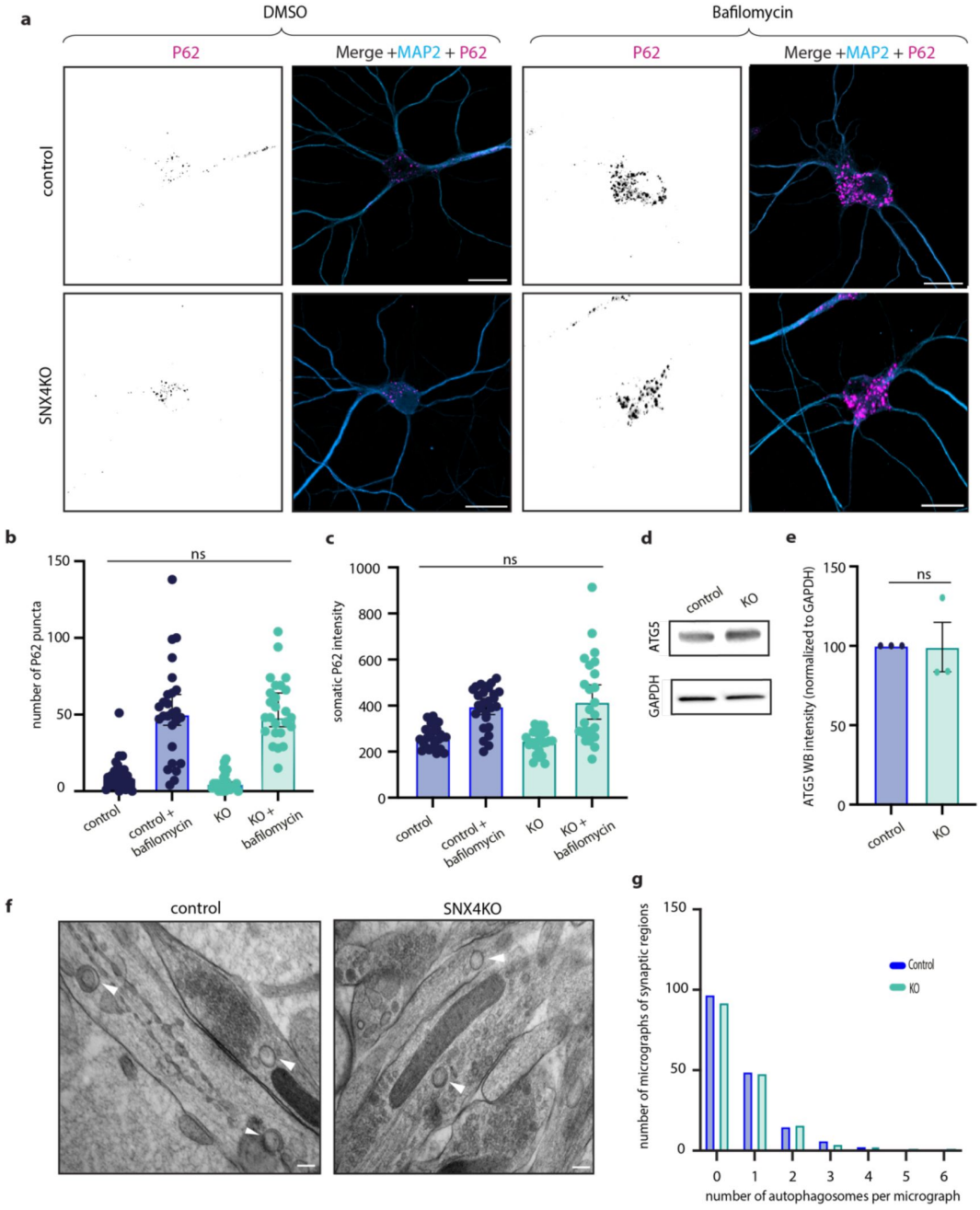

Supplementary 4

Autophagy markers remain unaffected upon SNX4 depletion.

(a) Typical example immunocytochemistry images of primary hippocampal neurons stained for P62 (magenta) and MAP2 (green) from control and SNX4 cKO mice with and without bafilomycin treatment. Scale bar = 20 µm. **(b)** P62 puncta control and KO. **(c)** P62 intensity measured in soma. **(d)** Western blot of ATG5 and actin for control and KO. **(e)** Quantification for total ATG5 expression levels normalized to GAPDH and control. **(f)** Typical example of autophagosomes characterized by double membrane in electron micrographs of control and KO. **(g)** Overview of number of micrographs of synaptic regions containing autophagosomes for control and KO. Bar graphs represent median with 95% CI. For (a,bc) n = 25-27 per group N=3, for (f-g) n = 165-170 photo's per group from N=3.

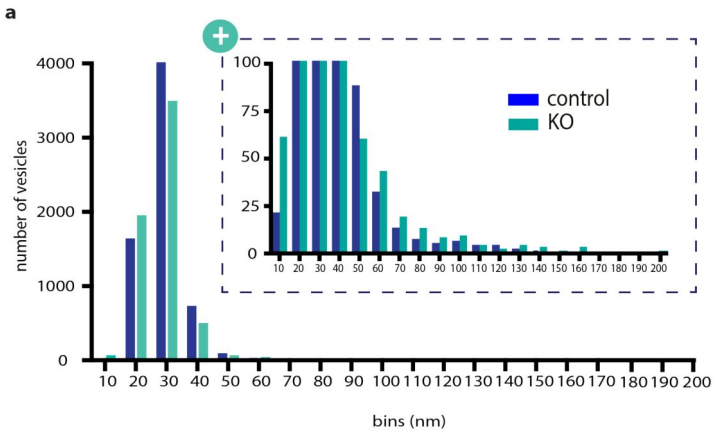

Supplementary 5

Histogram of vesicle size for control and SNX4KO synapses.

(a) Histogram of number of vesicles in bins per 10 nm.

Figure 1	n number (range neurons or synapses per group /animals)	mean	median	SEM	SD	significant test	p-value
snx4 wb	x/3	dcre = 100 21d cre = 9,913 18d cre = 16,87 14d cre = 32,52	dcre = 100 21d cre = 8,489 18d cre = 11,68 14d cre = 19,18	dcre = 0 21d cre = 4,943 18d cre = 9,817 14d cre = 25,52	dcre = 0 21d cre = 8,561 18d cre = 9,817 14d cre = 25,52	Ordinary one way anova	dcre-21d cre = 0,0003 dcre-18d cre = 0,0005 dcre-14d cre = 0,0019
snx4 fluorescence	38-42/6	control = 100,0 KO = 42,66	control = 98,74 KO = 37,46	control = 3,267 KO = 3,471	control = 21,17 KO = 21,40	mann-whitney test	p<0,0001
Dendrite length	32-36/6	control = 1530 KO = 1536	control = 1407 KO = 1389	control = 99,16 KO =109,6	control = 594,9 KO =620,2	mann-whitney test	p = 0,9077
# vamp2 puncta per neuron	35-41/6	control = 605,3 KO = 626,1	control = 536,0 KO =533,0	control = 40,23 KO =61,68	control = 257,6 KO = 364,9	mann-whitney test	p = 0,899
Figure 2							
Amplitude (pA)	25-34/4	control = 6081 KO = 7124 KO + SNX4 = 3508	control = 5272 KO = 6546 KO + SNX4 = 2908	control = 826,1 KO = 1076 KO + SNX4 = 439,6	control = 4817 KO =5382 KO + SNX4 = 2198	multilevel anova + bonferroni correction	Con-KO = 1 Con-SNX4 = 0,061 KO-SNX4 = 0,0378
Charge (pC)	25-33/4	control = 88,53 KO = 121,7 KO + SNX4 = 57,38	control = 66,98 KO = 78,04 KO + SNX4 = 40,06	control = 15,61 KO = 21,34 KO + SNX4 = 9,295	control = 89,67 KO = 106,7 KO + SNX4 = 47,40	multilevel anova + bonferroni correction	Con-KO = 0,7718 Con-SNX4 = 0,4833 KO-SNX4 = 0,0584
Inter pulse Ratio pulse 25 (p2/p1)	25-33/4	control = 0,9813 KO = 0,8808 KO + SNX4 = 1,022	control = 0,9489 KO = 0,8515 KO + SNX4 = 1,017	control = 0,06983 KO = 0,04791 KO + SNX4 = 0,06540	control = 0,4012 KO = 0,2395 KO + SNX4 = 0,3582	multilevel anova	p = 0,2756
Inter pulse Ratio pulse 50 (p2/p1)	15-19/4	control = 1,088 KO = 0,9564 KO + SNX4 = 1,152	control = 0,9337 KO = 0,9157 KO + SNX4 = 1,138	control = 0,09870 KO = 0,05315 KO + SNX4 = 0,08174	control = 0,3823 KO = 0,2126 KO + SNX4 = 0,3563	multilevel anova	p = 0,198
Inter pulse Ratio pulse 100 (p2/p1)	32-38/4	control = 0,9123 KO = 0,8791 KO + SNX4 = 0,9327	control = 0,8729 KO = 0,8553 KO + SNX4 = 0,9168	control = 0,03475 KO = 0,03696 KO + SNX4 = 0,04336	control = 0,2142 KO = 0,2024 KO + SNX4 = 0,2453	multilevel anova	p = 0,9329
Inter pulse Ratio pulse 200 (p2/p1)	25-29/4	control = 0,8399 KO = 0,8045 KO + SNX4 = 0,8718	control = 0,8257 KO = 0,7830 KO + SNX4 = 0,8747	control = 0,03448 KO = 0,02499 KO + SNX4 = 0,03094	control = 0,1857 KO = 0,1369 KO + SNX4 = 0,1547	multilevel anova	p = 0,3914
Average charge (pulse 90-100) (p2/p1)	25-33/4	control = 8,562 KO = 18,15 KO + SNX4 = 9,098	control = 6,557 KO = 9,282 KO + SNX4 = 4,745	control = 1,115 KO = 3,665 KO + SNX4 = 1,545	control = 6,405 KO = 18,33 KO + SNX4 = 8,318	multilevel anova + bonferroni correction	Con-KO = 0,0045 Con-SNX4 = 1 KO-SNX4 = 0,0067
RRP estimate (pC)	25-34/4	control = 783,5 KO = 871,7 KO + SNX4 = 659,3	control = 453,3 KO = 486,1 KO + SNX4 = 581,0	control = 167,2 KO = 158,9 KO + SNX4 = 93,64	control = 975,1 KO = 794,7 KO + SNX4 = 512,9	multilevel anova	p = 0,2124
slope estimate (pC/s)	25-33/4	control = 8,953 KO = 18,67 KO + SNX4 = 9,513	control = 7,074 KO = 9,569 KO + SNX4 = 5,667	control = 1,155 KO = 3,755 KO + SNX4 = 1,589	control = 6,636 KO = 18,78 KO + SNX4 = 8,555	multilevel anova + bonferroni correction	Con-KO = 0,0051 Con-SNX4 = 1 KO-SNX4 = 0,0073
mEPSCs amplitude	16-27/4-6	control = -31,83 KO = -30,75 KO + SNX4 = -30,78	control = -30,61 KO = -31,64 KO + SNX4 = -31,60	control = 1,580 KO = 1,407 KO + SNX4 = 1,351	control = 8,208 KO = 5,627 KO + SNX4 = 5,404	multilevel anova	p =0,7411
mEPSCs frequency	16-27/4-6	control = 1,965 KO = 1,855 KO + SNX4 = 1,975	control = 1,769 KO = 1,509 KO + SNX4 = 1,290	control = 0,2647 KO = 0,3627 KO + SNX4 =0,5250	control = 1,349 KO = 1,451 KO + SNX4 = 2,100	multilevel anova	p = 0,8694
Figure 3							
Stim1 (F/F0)	21-24/3	control = 0,5590 KO = 0,5028	control = 0,5382 KO = 0,4864	control = 0,03406 KO = 0,01363	control = 0,1669 KO = 0,06247	multilevel anova	p = 0.1643
Stim2 (F/F0)	21-24/3	control = 0,5663 KO = 0,5097	control = 0,5404 KO = 0,4768	control = 0,05318 KO = 0,02385	control = 0,2605 KO = 0,1093	multilevel anova	p = 0.4062
NH4 intensity	21-24/3	control = 2,002 KO = 1,507	control = 1,887 KO = 1,473	control = 0,1539 KO = 0,1268	control = 0,7538 KO = 0,5810	multilevel anova	p = 0.0152
release fraction first stim	21-24/3	control = 0,1928 KO = 0,2262	control = 0,1937 KO = 0,2031	control = 0,008183 KO =0,01943	control = 0,04009 KO = 0,08906	multilevel anova	*p = 0.0954*
release fraction 2nd stim	21-24/3	control = 0,1858 KO = 0,2206	control = 0,1781 KO = 0,1850	control = 0,01210 KO = 0,01976	control = 0,05929 KO = 0,09056	multilevel anova	p = 0.1195
decay time tau first stim	21-24/3	control = 1,606 KO = 1,919	control = 1,691 KO = 1,807	control = 0,6841 KO = 0,1571	control = 3,351 KO = 0,7201	multilevel anova	p = 0.6617
decay time tau second stim	21-24/3	control = 2,472 KO = 1,584	control = 1,721 KO = 1,400	control = 0,9126 KO = 0,1740	control = 4,471 KO = 0,7972	multilevel anova	p = 0.3612
average active synapses	21-24/3	control = 60,88 KO = 45,97	control = 66,76 KO = 47,46	control = 5,375 KO = 4,562	control =26,33 KO = 20,91	multilevel anova	p = 0.3127
FM4-64 release	28-36/4	control = 18,27 KO = 16,57	control = 15,04 KO = 15,71	control = 1,719 KO = 1,625	control = 10,32 KO = 8,600	multilevel anova	p = 0.5103
FM4-64 uptake	28-36/4	control = 100,0 KO = 94,27	control = 99,98 KO = 96,50	control = 3,263 KO = 4,586	control = 19,58 KO = 24,27	multilevel anova	p = 0.2882
Figure 5							
vamp2 puncta per um	35-41/6	control = 0,4829 KO = 0,5289	control = 0,4196 KO = 0,4486	control = 0,02679 KO = 0,03598	control = 0,1715 KO = 0,2128	mann-whitney test	p = 0,5053
vamp2 intensity in neurites	35-41/6	control = 100,0 KO = 92,94	control = 97,53 KO = 86,62	control = 3,505 KO = 5,445	control = 22,44 KO = 33,12	Unpaired t test with Welch's correction	p = 0,28
Figure 6							
fraction docked	174-175/3	control = 4,974 KO = 6,353	control = 4,487 KO = 5,556	control = 0,2251 KO = 0,2992	control = 2,978 KO = 3,946	mann-whitney test	p = 0,0002
# docked normalized to AZ	174-175/3	control = 0,9119377 KO = 1,390216	control = 0,8270241 KO = 1,404846	control = 0,02914 KO = 0,03772	control = 0,3854 KO = 0,4976	mann-whitney test	p < 0,0001
# docked ccv	174-175/3	control = 6,269 KO = 8,190	control = 6 KO = 7	control = 0,3017 KO = 0,3380	control = 3,992 KO = 4,458	mann-whitney test	p < 0,0001
# total ccv	174-175/3	control = 157,2 KO = 160,5	control = 120 KO = 134,5	control = 8,425 KO = 7,726	control = 111,5 KO = 101,9	mann-whitney test	p = 0,3682
vesicle size 0-50	174-175/3	control = 29,34 KO = 28,48	control = 28,50 KO = 27,39	control = 0,1007 KO = 0,1277	control = 8,186 KO = 10,02	multilevel anova	p = <,0001
vesicle size 0-50 per synapse	174-175/3	control = 27,54 KO = 28,48	control = 28,67 KO = 28,02	control = 0,2044 KO = 0,2427	control = 2,727 KO = 3,238	mann-whitney test	p = 0,0007
vesicle size 50 plus per synapse	174-175/3	control = 72,38 KO = 75,89	control = 67,19 KO = 65,95	control = 3,075 KO = 2,991	control = 22,17 KO = 22,18	mann-whitney test	p = 0,3529
vesicle cluster area	174-175/3	control = 0,2193 KO = 0,1741	control = 0,1720 KO = 0,1510	control = 0,01283 KO = 0,008008	control = 0,1697 KO = 0,1056	mann-whitney test	p = 0,0322
actie zone length	174-175/3	control = 706,1 KO = 600,3	control = 617,3 KO = 538,7	control = 29,98 KO = 21,17	control = 396,6 KO = 279,2	mann-whitney test	p = 0,0248
PSD length	174-175/3	control = 701,9 KO = 589,5	control = 611,4 KO = 526,8	control = 30,10 KO = 20,95	control = 398,2 KO = 276,4	mann-whitney test	p = 0,0157
Supplementary 3							
first evoked ampltidue (pA)	23-26/3	control = 4629 SNX4 OE = 4629	control = 4347 SNX4 OE = 3217	control = 602,9 SNX4 OE = 775,5	control = 3074 SNX4 OE = 3719	multilevel anova + bonferroni correction	p = 0,81
first evoked charge (pC)	22-25/3	control = 48,73 SNX4 OE = 39,49	control = 43,36 SNX4 OE = 27,80	control = 6,558 SNX4 OE = 7,631	control = 32,79 SNX4 OE = 35,79	multilevel anova + bonferroni correction	p = 0,361
Average charge (pulse 90-100) (p2/p1)	21-25/3	control = 9,228 SNX4 OE = 12,17	control = 6,229 SNX4 OE = 8,734	control = 1,474 SNX4 OE = 3,193	control = 7,372 SNX4 OE = 14,63	multilevel anova	p = 0.787
Supplementary 4							
number of P62 puncta	25-27/3	control = 10,76 control +bafilomycin = 51,88 KO = 5,960 KO +bafilomycin = 53,24	control = 9,000 control +bafilomycin = 50,00 KO = 4,000 KO +bafilomycin = 48,00	control = 2,120 control +bafilomycin = 6,134 KO = 1,220 KO +bafilomycin = 4,137	control = 10,60 control +bafilomycin = 31,28 KO = 6,100 KO +bafilomycin = 20,68	Kruskall-Wallis Dunn's multilple comparison	p = >0.9999
somatic P62 intensity	25-27/3	control = 263,8 control +bafilomycin = 396,3 KO = 247,3 KO +bafilomycin = 415,6	control = 262,0 control +bafilomycin = 411,3 KO = 246,1 KO +bafilomycin = 360,8	control = 9,745 control +bafilomycin = 17,08 KO = 10,19 KO +bafilomycin = 36,19	control = 48,73 control +bafilomycin = 88,75 KO = 50,94 KO +bafilomycin = 181,0	Kruskall-Wallis Dunn's multilple comparison	p = >0.9999
ATG5 WB levels	3	control = 100,0 KO = 99,23	control = 100,0 KO = 83,89	control = 0 KO = 15,54	control = 0 KO = 26,92	Unpaired t test	p = 0,9628

Supplementary table 1

Statistics overview

References

Aarts E., Verhage M., Veenvliet J. V., Dolan C. V., Van Der Sluis S. (2014) **A solution to dependency: using multilevel analysis to accommodate nested data** *Nature Neuroscience* **17**:491–496 https://doi.org/10.1038/NN.3648

Antón Z., Betin V. M. S., Simonetti B., Traer C. J., Attar N., Cullen P. J., Lane J. D (2020) **A heterodimeric SNX4–SNX7 SNX-BAR autophagy complex coordinates ATG9A trafficking for efficient autophagosome assembly** *Journal of Cell Science* **133** https://doi.org/10.1242/jcs.246306

Carlton J., Bujny M., Rutherford A., Cullen P (2005) **Sorting nexins--unifying trends and new perspectives. Traffic (Copenhagen** *Denmark* **6**:75–82 https://doi.org/10.1111/J.1600-0854.2005.00260.X

Ceccarelli B., Hurlbut W. P., Mauro A (1973) **Turnover of Transmitter and Synaptic Vesicles at the Frog Neuromuscular Junction** *Journal of Cell Biology* **57**:499–524 https://doi.org/10.1083/JCB.57.2.499

Chen X., Ma W., Zhang S., Paluch J., Guo W., Dickman D. K (2017) **The BLOC-1 Subunit Pallidin Facilitates Activity-Dependent Synaptic Vesicle Recycling** *Eneuro* **4** https://doi.org/10.1523/ENEURO.0335-16.2017

Chen X. W. *et al.* (2008) **DTNBP1, a schizophrenia susceptibility gene, affects kinetics of transmitter release** *Journal of Cell Biology* **181**:791–801 https://doi.org/10.1083/jcb.200711021

Cullen P. J., Steinberg F (2018) **To degrade or not to degrade: mechanisms and significance of endocytic recycling** *Nature Reviews Molecular Cell Biology* **19**:679–696 https://doi.org/10.1038/s41580-018-0053-7

Decet M., Verstreken P (2021) **Presynaptic Autophagy and the Connection With Neurotransmission** *Frontiers in Cell and Developmental Biology* **9** https://doi.org/10.3389/FCELL.2021.790721

Dörrbaum A. R., Kochen L., Langer J. D., Schuman E. M (2018) **Local and global influences on protein turnover in neurons and glia** *ELife* **7** https://doi.org/10.7554/ELIFE.34202

Fernandes A. C., Uytterhoeven V., Kuenen S., Wang Y.-C., Slabbaert J. R., Swerts J., Kasprowicz J., Aerts S., Verstreken P (2014) **Reduced synaptic vesicle protein degradation at lysosomes curbs TBC1D24/sky-induced neurodegeneration** *The Journal of Cell Biology* **207**:453–462 https://doi.org/10.1083/jcb.201406026

Granseth B., Odermatt B., Royle S. J. J., Lagnado L (2006) **Clathrin-mediated endocytosis is the dominant mechanism of vesicle retrieval at hippocampal synapses** *Neuron* **51**:773–786 https://doi.org/10.1016/J.NEURON.2006.08.029

Hanley S. E., Willis S. D., Cooper K. F (2021) **Snx4-assisted vacuolar targeting of transcription factors defines a new autophagy pathway for controlling ATG expression** *Autophagy* **17** https://doi.org/10.1080/15548627.2021.1877934

Hettema E. H., Lewis M. J., Black M. W., Pelham H. R. B (2003) **Retromer and the sorting nexins Snx4/41/42 mediate distinct retrieval pathways from yeast endosomes** *EMBO Journal* **22**:548–557 https://doi.org/10.1093/emboj/cdg062

Heuser E., Reese T. S (1973) **Evidence for Recycling of Synaptic Vesicle Membrane during Transmitter Release at the Frog Neuromuscular Junction** *The Journal of Cell Biology* **57**:15–344

Huotari J., Helenius A (2011) **Endosome maturation** *The EMBO Journal* **30**:3481–3500 https://doi.org/10.1038/EMBOJ.2011.286

Inoshita T. *et al.* (2017) **Vps35 in cooperation with LRRK2 regulates synaptic vesicle endocytosis through the endosomal pathway in Drosophila** *Human Molecular Genetics* **26**:2933–2948 https://doi.org/10.1093/hmg/ddx179

Kaeser P. S., Deng L., Wang Y., Dulubova I., Liu X., Rizo J., Südhof T. C (2011) **RIM proteins tether Ca2+ channels to presynaptic active zones via a direct PDZ-domain interaction** *Cell* **144**:282–295 https://doi.org/10.1016/j.cell.2010.12.029

Kim N. Y., Cho M. H., Won S. H., Kang H. J., Yoon S. Y., Kim D. H (2017) **Sorting nexin-4 regulates β-amyloid production by modulating β-site-activating cleavage enzyme-1** *Alzheimer's Research and Therapy* **9** https://doi.org/10.1186/s13195-016-0232-8

Kononenko N. L., Haucke V. (2015) **Molecular mechanisms of presynaptic membrane retrieval and synaptic vesicle reformation** *Neuron* Cell Press :484–496 https://doi.org/10.1016/j.neuron.2014.12.016

Kuijpers M., Kochlamazashvili G., Stumpf A., Puchkov D., Swaminathan A., Lucht M. T., Krause E., Maritzen T., Schmitz D., Haucke V (2021) **Neuronal Autophagy Regulates Presynaptic Neurotransmission by Controlling the Axonal Endoplasmic Reticulum** *Neuron* **109**:299–313 https://doi.org/10.1016/J.NEURON.2020.10.005

Kusick G. F., Chin M., Raychaudhuri S., Lippmann K., Adula K. P., Hujber E. J., Vu T., Davis M. W., Jorgensen E. M., Watanabe S (2020) **Synaptic vesicles transiently dock to refill release sites** *Nature Neuroscience* **23**:1329–1338 https://doi.org/10.1038/s41593-020-00716-1

Ma M., Burd C. G., Chi R. J (2017) **Distinct complexes of yeast Snx4 family SNX-BARs mediate retrograde trafficking of Snc1 and Atg27. Traffic (Copenhagen** *Denmark* **18** https://doi.org/10.1111/TRA.12462

Moro A., van Nifterick A., Toonen R. F., Verhage M. (2021) **Dynamin controls neuropeptide secretion by organizing dense-core vesicle fusion sites** *Science Advances* **7**:659–680

Naldini L., Blömer U., Gallay P., Ory D., Mulligan R., Gage F. H., Verma I. M., Trono D (1996) **In Vivo Gene Delivery and Stable Transduction of Nondividing Cells by a Lentiviral Vector** *Science* **272**:263–267 https://doi.org/10.1126/SCIENCE.272.5259.263

Neher E (2015) **Merits and Limitations of Vesicle Pool Models in View of Heterogeneous Populations of Synaptic Vesicles** *Neuron* **87**:1131–1142 https://doi.org/10.1016/J.NEURON.2015.08.038

Rizzoli S. O (2014) **Synaptic vesicle recycling: steps and principles** *The EMBO Journal* **33** https://doi.org/10.1002/EMBJ.201386357

Sardana R., Emr S. D (2021) **Membrane Protein Quality Control Mechanisms in the Endo-Lysosome System** *Trends in Cell Biology* **31**:269–283 https://doi.org/10.1016/J.TCB.2020.11.011

Schmitz S. K. *et al.* (2011) **Automated analysis of neuronal morphology, synapse number and synaptic recruitment** *Journal of Neuroscience Methods* **195**:185–193 https://doi.org/10.1016/J.JNEUMETH.2010.12.011

Schneggenburger R., Meyer A. C., Neher E (1999) **Released fraction and total size of a pool of immediately available transmitter quanta at a calyx synapse** *Neuron* **23**:399–409 https://doi.org/10.1016/S0896-6273(00)80789-8

Schoch S., Deák F., Königstorfer A., Mozhayeva M., Sara Y., Südhof T. C., Kavalali E. T (2001) **SNARE function analyzed in synaptobrevin/VAMP knockout mice** *Science* **294**:1117–1122 https://doi.org/10.1126/science.1064335

Simonetti B., Daly J. L., Cullen P. J (2023) **Out of the ESCPE room: Emerging roles of endosomal SNX-BARs in receptor transport and host–pathogen interaction** *Traffic* **24**:234–250 https://doi.org/10.1111/TRA.12885

Soykan T., Haucke V., Kuijpers M (2021) **Mechanism of synaptic protein turnover and its regulation by neuronal activity** *Current Opinion in Neurobiology* **69**:76–83 https://doi.org/10.1016/J.CONB.2021.02.006

Südhof T. C (2000) **The synaptic vesicle cycle revisited** *Neuron* **28**:317–320 https://doi.org/10.1016/S0896-6273(00)00109-4

Sugatha J., Priya A., Raj P., Jaimon E., Swaminathan U., Jose A., Pucadyil T. J., Datta S (2023) **Insights into cargo sorting by SNX32 and its role in neurite outgrowth** *ELife* **12** https://doi.org/10.7554/eLife.84396

Tagliatti E., Fadda M., Falace A., Benfenati F., Fassio A. (2016) **Arf6 regulates the cycling and the readily releasable pool of synaptic vesicles at hippocampal synapse** *ELife* **5**:1–18 https://doi.org/10.7554/eLife.10116

Teasdale R. D., Loci D., Houghton F., Karlsson L., Gleeson P. A (2001) **A large family of endosome-localized proteins related to sorting nexin 1** *The Biochemical Journal* **358**:7–16 https://doi.org/10.1042/0264-6021:3580007

Toh W. H., Cheryl Chia P. Z., Iqbal Hossain M., Gleeson P. A (2018) **GGA1 regulates signal-dependent sorting of BACE1 to recycling endosomes, which moderates Aβ production** *Molecular Biology of the Cell* **29** https://doi.org/10.1091/MBC.E17-05-0270

Traer C. J., Rutherford A. C., Palmer K. J., Wassmer T., Oakley J., Attar N., Carlton J. G., Kremerskothen J., Stephens D. J., Cullen P. J (2007) **SNX4 coordinates endosomal sorting of TfnR with dynein-mediated transport into the endocytic recycling compartment** *Nature Cell Biology* **9**:1370–1380 https://doi.org/10.1038/ncb1656

Truckenbrodt S., Viplav A., Jähne S., Vogts A., Denker A., Wildhagen H., Fornasiero E. F., Rizzoli S. O (2018) **Newly produced synaptic vesicle proteins are preferentially used in synaptic transmission** *The EMBO Journal* **37**:1–24 https://doi.org/10.15252/embj.201798044

Uytterhoeven V., Kuenen S., Kasprowicz J., Miskiewicz K., Verstreken P (2011) **Loss of Skywalker reveals synaptic endosomes as sorting stations for synaptic vesicle proteins** *Cell* **145**:117–132 https://doi.org/10.1016/j.cell.2011.02.039

Van Weering J. R. T., Sessions R. B., Traer C. J., Kloer D. P., Bhatia V. K., Stamou D., Carlsson S. R., Hurley J. H., Cullen P. J. (2012) **Molecular basis for SNX-BAR-mediated assembly of distinct endosomal sorting tubules** *EMBO Journal* **31**:4466–4480 https://doi.org/10.1038/emboj.2012.283

van Weering J. R. T., Verkade P., Cullen P. J. (2012) **SNX–BAR-Mediated Endosome Tubulation is Co-ordinated with Endosome Maturation** *Traffic* **13**:94–107 https://doi.org/10.1111/J.1600-0854.2011.01297.X

Vazquez-Sanchez S., Gonzalez-Lozano M. A., Walfenzao A., Li K. W., van Weering J. R. T. (2020) **The endosomal protein sorting nexin 4 is a synaptic protein** *Scientific Reports* **10** https://doi.org/10.1038/s41598-020-74694-6

Vietri M., Radulovic M., Stenmark H (2020) **The many functions of ESCRTs** *Nature Reviews. Molecular Cell Biology* **21**:25–42 https://doi.org/10.1038/S41580-019-0177-4

Watanabe S., Boucrot E (2017) **Fast and ultrafast endocytosis** *Current Opinion in Cell Biology* **47**:64–71 https://doi.org/10.1016/J.CEB.2017.02.013

Watanabe S., Rost B. R., Camacho-Pérez M., Davis M. W., Söhl-Kielczynski B., Rosenmund C., Jorgensen E. M (2013) **Ultrafast endocytosis at mouse hippocampal synapses** *Nature* **504**:242–247 https://doi.org/10.1038/nature12809

Zhou C. *et al.* (2022) **Recycling of autophagosomal components from autolysosomes by the recycler complex** *Nature Cell Biology* **24**:497–512 https://doi.org/10.1038/s41556-022-00861-8

Author information

Josse Poppinga

Department of Functional Genomics, Center for Neurogenomics and Cognitive Research (CNCR), VU University, Amsterdam, The Netherlands

Nolan J Barret

Department of Functional Genomics, Center for Neurogenomics and Cognitive Research (CNCR), VU University, Amsterdam, The Netherlands

L Niels Cornelisse

Department of Functional Genomics, Center for Neurogenomics and Cognitive Research (CNCR), VU University, Amsterdam, The Netherlands, Department of Human Genetics, CNCR, Amsterdam UMC, Amsterdam, The Netherlands

Matthijs Verhage

Department of Functional Genomics, Center for Neurogenomics and Cognitive Research (CNCR), VU University, Amsterdam, The Netherlands, Department of Human Genetics, CNCR, Amsterdam UMC, Amsterdam, The Netherlands
ORCID iD: 0000-0002-6085-7503

Jan RT van Weering

Department of Functional Genomics, Center for Neurogenomics and Cognitive Research (CNCR), VU University, Amsterdam, The Netherlands, Department of Human Genetics, CNCR,

Amsterdam UMC, Amsterdam, The Netherlands
ORCID iD: 0000-0001-5259-4945

For correspondence: jan.van.weering@vu.nl

Editors

Reviewing Editor
Rafael Fernández-Chacon
Instituto de Biomedicina de Sevilla (IBiS), Sevilla, Spain

Senior Editor
Lu Chen
Stanford University, Stanford, United States of America

Reviewer #1 (Public review):

Summary:

In the work Josse Poppinga and collaborators addressed the synaptic function of Sortin-Nexin 4 (SNX4). Employing a newly-developed in vitro KO model, with live imaging experiments, electrophysiological recordings and ultrastructural analysis, the authors evaluate modifications in synaptic morphology and function upon loss of SNX4. The data demonstrate increased neurotransmitter release and alteration in synapse ultrastructure with higher number of docked vesicles and shorter AZ. The evaluation of presynaptic function of SNX4 is of relevance and tackles an open and yet unresolved question in the field of presynaptic physiology.

Strengths:

The sequential characterization of the cellular model is nicely conducted, and the different techniques employed are appropriate for the morpho-functional analysis of the synaptic phenotype and the derived conclusions on SNX4 function at presynaptic site. The authors succeeded in presenting a novel in vitro model that results in chronic deletion of SNX4 in neurons. A convincing sequence of experimental techniques are applied to the model to unravel the role of SNX4, whose functions in neuronal cells and at synapses are largely unknown. The understanding of the role of endosomal sorting at presynaptic site is relevant and of high interest in the field of synaptic physiology and on the pathophysiology of the many described synaptopathies that broadly result in loss of synaptic fidelity and quality control at release sites.

Weaknesses:

The flow of the data presentation is mostly descriptive with several consistent morphological and functional modifications upon SNX loss. The paper would benefit from a wider characterization that would allow to address the physiological roles of SNX4 at synaptic site and speculate on the underlying molecular mechanisms. The novel experiments on autophagy progression as well as spontaneous neurotransmission are well conducted, although do not assist for the explanation of the molecular mechanism underneath.

Comments on revisions:

Other implementations in the revised version are quite limited and would benefit from a more detailed presentation and description. i.e.: Sholl analysis in the new figure 1h, is presented with no definition of number of cells employed and standard deviations of the replication. The "simil" Sholl analysis performed on VAMP2 is still puzzling and some

explanations on the reason for the constant value of VAMP2 fluorescent signal from less than 0 to 160 μm from the cell body is to be added. How is the increased number of active synapses explained? How is this related to shorter AZ and higher number of docked vesicles?

https://doi.org/10.7554/eLife.97910.2.sa3

Reviewer #2 (Public review):

Summary:

SNX4 is thought to mediate recycling from endosomes back to the plasma membrane in cells. In this study, the authors demonstrate the increases in the amounts of transmitter release and the number of docked vesicles by combining genetics, electrophysiology and EM. They failed to find evidence for its role in synaptic vesicle cycling and endocytosis, which may be intuitively closer to the endosome function.

Strengths:

The electrophysiological data and EM data are in principle, convincing, though there are several issues in the study.

Weaknesses:

It is unclear why the increase in the amounts of transmitter release and docked vesicles happened in the SNX4 KO mice. In other words, it is unclear how the endosomal sorting proteins in the end regulate or are connected to presynaptic, particularly the active zone function.

Comments on revisions:

I am fine with revision in principle. the authors have addressed my concerns.

https://doi.org/10.7554/eLife.97910.2.sa2

Reviewer #3 (Public review):

Summary:

The study aims to determine whether the endosomal protein SNX4 performs a role in neurotransmitter release and synaptic vesicle recycling. The authors exploited a newly generated conditional knockout mouse to allow them to interrogate SNX4 function. A series of basic parameters were assessed, with an observed impact on neurotransmitter release and active zone morphology. The work is interesting, however as things currently stand, the work is descriptive with little mechanistic insight. There are a number of places where some of the conclusions require further validation.

Strengths:

The strengths of the work are the state-of-the-art methods to monitor presynaptic function.

Weaknesses:

The weaknesses are the fact that the work is largely descriptive, with no mechanistic insight into the role of SNX4.

Comments on revisions:

The authors have addressed a couple of the more major concerns with the manuscript, however many of the original weaknesses remain. The primary weakness being the lack of mechanism. It is disappointing that real-time VAMP2 trafficking was not investigated, and the authors justification as to why the experiment was not performed was not convincing (especially since this is the approach that all other groups employ to examine SV cargo trafficking). In a number of instances "contractual constraints" are referred to as an explanation for not performing additional experiments. It was unclear whether this refers to licencing issues with the mouse line or the lack of personnel to perform the work. Regardless it still leaves this work as somewhat incomplete.

https://doi.org/10.7554/eLife.97910.2.sa1

Author response:

The following is the authors' response to the original reviews.

> ***Public Reviews:***
>
> ***Reviewer #1 (Public Review):***
>
> *Summary:*
>
> *In the work: "Endosomal sorting protein SNX4 limits synaptic vesicle docking and release" Josse Poppinga and collaborators addressed the synaptic function of Sortin-Nexin 4 (SNX4). Employing a newly developed in vitro KO model, with live imaging experiments, electrophysiological recordings, and ultrastructural analysis, the authors evaluate modifications in synaptic morphology and function upon loss of SNX4. The data demonstrate increased neurotransmitter release and alteration in synapse ultrastructure with a higher number of docked vesicles and shorter AZ. The evaluation of the presynaptic function of SNX4 is of relevance and tackles an open and yet unresolved question in the field of presynaptic physiology.*
>
> *Strengths:*
>
> *The sequential characterization of the cellular model is nicely conducted and the different techniques employed are appropriate for the morpho-functional analysis of the synaptic phenotype and the derived conclusions on SNX4 function at presynaptic site. The authors succeeded in presenting a novel in vitro model that resulted in chronical deletion of SNX4 in neurons. A convincing sequence of experimental techniques is applied to the model to unravel the role of SNX4, whose functions in neuronal cells and at synapses are largely unknown. The understanding of the role of endosomal sorting at the presynaptic site is relevant and of high interest in the field of synaptic physiology and in the pathophysiology of the many described synaptopathies that broadly result in loss of synaptic fidelity and quality control at release sites.*

We thank the reviewer for their positive evaluation of our manuscript.

> *Weaknesses:*
>
> *The flow of the data presentation is mostly descriptive with several consistent morphological and functional modifications upon SNX loss. The paper would benefit from a wider characterization that would allow us to address the physiological roles of SNX4 at the synaptic site and speculate on the underlying molecular mechanisms. In addition, due to the described role of SNX4 in autophagy and the high interest in the regulation of synaptic autophagy in the field of synaptic physiology, an initial evaluation*

> *of the autophagy phenotype in the neuronal SNX4KO model is important, and not to be only restricted to the discussion section.*

We thank the reviewer for their suggestions and agree that broader characterization would help us speculate on the underlying mechanism. To address this, we have conducted additional independent experiments investigating the role of SNX4 in neuronal autophagy, as suggested by this reviewer. These experiments are now included in the main figures and are no longer limited to the discussion section. Please see the detailed responses to this reviewer's recommendations below.

> ***Reviewer #2 (Public Review):***
>
> *Summary:*
>
> *SNX4 is thought to mediate recycling from endosomes back to the plasma membrane in cells. In this study, the authors demonstrate the increases in the amounts of transmitter release and the number of docked vesicles by combining genetics, electrophysiology, and EM. They failed to find evidence for its role in synaptic vesicle cycling and endocytosis, which may be intuitively closer to the endosome function.*
>
> *Strengths:*
>
> *The electrophysiological data and EM data are in principle, convincing, though there are several issues in the study.*

We thank the reviewer for their positive evaluation of our manuscript.

> *Weaknesses:*
>
> *It is unclear why the increase in the amounts of transmitter release and docked vesicles happened in the SNX4 KO mice. In other words, it is unclear how the endosomal sorting proteins in the end regulate or are connected to presynaptic, particularly the active zone function.*

We thank the reviewer for their suggestions and agree that further characterization would help to understand how endosomal sorting proteins regulate presynaptic neurotransmission. We have now added extra data on electrophysiological recordings clarifying SNX4's role in the synapse. Please see the detailed responses to this reviewer's recommendations below.

> ***Reviewer #3 (Public Review):***
>
> *Summary:*
>
> *The study aims to determine whether the endosomal protein SNX4 performs a role in neurotransmitter release and synaptic vesicle recycling. The authors exploited a newly generated conditional knockout mouse to allow them to interrogate the SNX4 function. A series of basic parameters were assessed, with an observed impact on neurotransmitter release and active zone morphology. The work is interesting, however as things currently stand, the work is descriptive with little mechanistic insight. There are a number of places where the data appear to be a little preliminary, and some of the conclusions require further validation.*
>
> *Strengths:*
>
> *The strengths of the work are the state-of-the-art methods to monitor presynaptic function.*

We thank the reviewers for their positive evaluation of our manuscript.

> *Weaknesses:*
>
> *The weaknesses are the fact that the work is largely descriptive, with no mechanistic insight into the role of SNX4. Further weaknesses are the absence of controls in some experiments and the design of specific experiments.*

We thank the reviewer for their suggestions and agree that addition of extra control groups and experiments would strengthen interpretation of the observed phenotype. To address this, we have now performed experiments to investigate the miniature excitatory postsynaptic currents and added extra control groups such as overexpression of SNX4 on control background. In addition, we assessed SNX4-mediated neuronal autophagy as a potential molecular mechanism by which SNX4 affects synaptic output. Please see the detailed responses to this reviewers' recommendations below.

> ***Recommendations for the authors:***
>
> ***Reviewer #1 (Recommendations For The Authors):***
>
> *(1) The characterization of the neurite outgrowth presented in Figure 1 is a necessary starting point for the characterization of the model and the interpretation of the following data. Being the analysis conducted at 21 DIV, a significant portion of the neurite tree is out of the analyzed field. Adding sholl analysis will better indicate the complexity of the that appears to be influenced by SNX4 loss in the representative images shown in Figure 1f.*

We fully agree and have now performed a Sholl analysis of dendrite branches to investigate dendritic complexity. (Figure 1(i), page 2-3, line 86-88). SNX4 depletion does not affect dendrite length or dendrite branching.

> *(2) Analogously, the characterization of synapse number is of relevance for the interpretation of the data. For a better flow of the data, Figure 4 might be presented as Figure 2 (without the repetition of panel h in Figure 1). An explanation of how VAMP2 puncta are processed is necessary in the method section. A double labelling with a postsynaptic marker would allow trafficking organelles to be distinguished from mature synaptic contacts. Indeed, the analysis of VAMP2 intensity along neurite in mature 21DIV neurons should reveal peaks in the intensity profile that represent synaptic contacts. For unexplained reasons, the profile is rather flat in the two experimental groups. Focusing on axonal branches will surely result in a peaked profile for VAMP2 labelling.*

We fully agree that the characterization of synapses is relevant for the interpretation of the data. We have now added a section in our Material and Methods how the VAMP2 puncta are processed (p14 line 517-520). Instead of labeling mature synapses using double labeling of VAMP2 and PSD95, we analyzed the number of active synapses in live neurons using SypHy (Fig. 3g). The reviewer is correct that the VAMP2 data presented in Fig 1I and Fig 4 is part of the same dataset and we have clarified this in the figure legend. In Fig 1I only the total number of VAMP2 puncta is plotted as a marker for synapse number, while in Fig 4 we assess VAMP2 as potential SNX4 sorting cargo (Ma et al., 2017). Because of these different aims, we prefer to keep the figures separate. The analysis of VAMP2 intensity along the distance of the soma is a Sholl analysis (Fig. 4d), represents the average VAMP2 intensity over distance from the soma of 35-41 neurons per group. In contrast to a line scan of a single neurite, this average profile lacks the peaks of individual synapses.

> *(3) Miniature excitatory postsynaptic currents recordings would strengthen the synaptic characterization and complement the electrophysiological recordings shown in Figure 2. Analyzing frequency and amplitude parameters would complement the data on the number of synaptic connections defined by the pre and postsynaptic colocalization puncta as suggested above and may support the data shown in Figure 3 g that suggests a decreased number of active synapses in SNX4-KO cells.*

We fully agree that the characterization of miniature excitatory postsynaptic currents would strengthen the synaptic characterization and complement the other electrophysiological data. Therefore, we have now added additional experiments showing the mEPSCs (Fig. 2k-m, page 4) in SNX4 cKO neurons versus control. This data shows that the amplitude and frequency of spontaneous miniature EPSCs (mEPSCs) were not affected upon SNX4 depletion, consistent with a normal first evoked EPSC and RRP estimate. Furthermore, these data suggest that it is unlikely that the observed increase in neurotransmission is due to post-synaptic effects.

> *(4) Recordings on the first evoked response shown in Figure 2 b and quantified in Figures c and d suggest that SNX4 overexpression per se exerts some effect on the Amplitude and the Charge of the first evoked response. This is also evident in the supplementary Figure 2 with lower frequency trains. An additional experimental group, namely control+SNX4 is needed for the correct interpretation of the observed phenotype. The possibility that SNX4 per se exerts an effect on evoked transmission could be discussed in terms of putative mechanisms and interactions.*

We thank the reviewer for their suggestion and agree that an additional experimental group (control + SNX4) would strengthen interpretation of the observed phenotype. We have now added a new experimental condition with overexpression of SNX4 on a control background (Supplementary Fig. 3, page 20). This data shows that the amplitude and charge of the first evoked response were not affected in control + SNX4 neurons compared to control, and no differences were detected in the response to the 40 Hz stimulation train (Supplementary Fig. 3a-e). Together, these data suggest that SNX4 overexpression in itself does not affect the neurotransmission protocols studied in SNX4 cKO experiments.

> *(5) To correctly interpret the SyPhy experiments and exclude an effect of SNX silencing on SV recycling, it is suggested to repeat the experiments shown in Figure 3 in the absence and in the presence of bafilomycin. Indeed, the quantifications shown in Figure 3 d and f do not represent "release fraction" as stated (lines 139/140) but they rather refer to an average difference between release fraction and recovered fraction. With the use of bafilomycin, the comparison of the deltaFmax/deltaFNH4Cl with and without bafilomycin would enable the release fraction to be correctly evaluated and compared.*

We appreciate the reviewer's suggestion and agree on the importance of considering the impact of SV recycling when evaluating the released fraction. We agree that the presence of bafilomycin is critical to isolate the released component during stimulation. We have now rephrased this conclusion. To assess synaptic recycling in these assays, bafilomycin in not critically required and we show by multiple independent experiments, including SypHy and FM64 dye assays, that SV recycling is either not affected or the effect is too small to be detected by these methods.

> *(6) In the ultrastructural analysis, additional quantifications are needed to exclude the accumulation of endosome-like structures. It is not clear if, in the evaluation of total SV number (Figure 5e), the authors counted all vesicles or vesicles < 50nm. This has to be explained and additional quantification of # of SV < 50nm and # SV > 50nm is informative, taking into account the endosomal nature of SNX4. Indeed, although the*

> *average size of SV is not changed (fig. 5 d), the density of "bigger vesicle" may result from endosomal-like structure accumulation. An additional suggested quantification is on vesicle # SV > 80nm as previously reported in the cited references dealing with endosomal proteins and presynaptic morphology.*

We fully agree that the characterization of vesicle size is important and that it was not clearly stated which vesicles were included in the total number of SV (Fig. 5e). We have now added this to the figure description. We have also added a histogram that contains the vesicle numbers of different bin sizes for SNX4 cKO synapses and control synapses (Supplementary Fig. 4, page 21) including # SVs > 80nm. (Whilst it seems that there are more “bigger” vesicles in the KO, further analysis revealed that this is mostly driven by one experiment and this effect is not consistent.)

> *(7) Due to the high scientific interest in presynaptic autophagy for SV recycling and degradation, and the paucity of experimental work assessing the proteins involved, an initial evaluation of the neuronal autophagy process (by western blot analysis and immunocytochemistry) for the characterization of the model will better support the paragraph in the discussion (lines 314-322) and contribute to future work in the field. Although very rare, autophagosomes quantification at presynaptic sites can also be performed from the already acquired images. A double membrane structure with the material inside is evident in the representative control image presented!*

We appreciate the reviewer’s suggestion and agree that presynaptic autophagy is an interesting potential mechanism that would elaborate our current working model. To address the reviewers’ suggestion, we added multiple independent experiments to investigate basal autophagy markers such as ATG5 using western blot analysis, characterization of p62 levels using immunohistochemistry and performed additional morphometric analysis on the electron microscopy data (Supplementary Fig. 5). In SNX4 cKO neurons, there was no significant difference in P62 puncta numbers or P62 somatic intensity under basal conditions or after blocking autophagic P62 degradation by bafilomycin treatment, suggesting that autophagic flux remains normal. Also, no changes in total ATG5 protein levels were observed and ultrastructural analysis revealed no differences in the total number of autophagosomes. Collectively, these data indicate that SNX4 depletion does not impact the basal autophagic flux, ATG5 protein levels, or the number of autophagosomes.

> *Minor points:*
>
> *(1) Dorrbaun et al. 2018 is missing from the reference list. In the legend to figure 1 there is an incorrect reference to Figure 6, rather than Figure 4.*

We have now adjusted the figure legend and added the reference (page 16, line 604).

> *(2) Information on the construct employed for the rescue is missing. Is it a fluorescent tag construct? Representative images of the three autaptic neurons (control, KO, KO+SNX4) would nicely complement data presentation in Figure 2.*

We have now elaborated on this in material and methods section (p12, line 418-421). Unfortunately, we did not obtain pictures of autaptic neurons used for electrophysiology experiments.

> ***Reviewer #2 (Recommendations For The Authors):***
>
> *(1) Figure 2d and f are somewhat inconsistent. Total charges for the 1st EPSCs differ almost 2-fold in the same condition.*

We appreciate the reviewer's concern. The average EPSCs charge of the first evoked was 89, 122 and 57 pC for control, KO and rescued neurons respectfully. The average charge of the first pulse of 40Hz train was 41,58 and 32 pC for control, KO and rescued neurons respectfully, which is roughly 50% of the naïve response of the same cells. These trains were recorded after 2 or 3 other stimulation paradigms, which can have affected the total charge released in the 40Hz train. That said, the proportional difference between groups is high comparable, with a 37% increased average charge released in SNX4 cKO compared to control in the naïve response and 41% increased response in the first response of the 40 Hz train, and rescued cells show a 53% reduction in average released charge compared to control in the naïve response compared to a 44% reduction in the first response of the 40 Hz train. Although the absolute values differ between these readouts, we conclude that the biological comparison between groups is consistent.

> *(2) Figure 2h. This type of analysis has a drawback. See Neher (2015) for the problems associated with this analysis.*

We fully agree with the reviewer's comment. As noted in our discussion (page 9 line 285), while this analysis has its limitations, it can still provide an indication of the ready releasable pool.

> *(3) The EPSC phenotype may be due to postsynaptic effects. This should be excluded by additional experiments (mEPSC analysis) or further clarification.*

We fully agree that the characterization of miniature excitatory postsynaptic currents recording would strengthen the synaptic characterization and complement the electrophysiological recordings. Therefore, we have now added additional experiments showing the mEPSCs (Fig. 2k-m) in SNX4 cKO neurons versus control. This data shows that the amplitude and frequency of spontaneous miniature EPSCs (mEPSCs) were not affected upon SNX4 depletion, suggesting that it is unlikely that the observed increase in neurotransmission is due to post-synaptic effects.

> *(4) The increased number of docked vesicles observed in EM and the increased slope (vesicle recruitment, Figure 2h) are not consistent with each other. Maybe the definition of docked vesicles is unclear in this version of the manuscript.*

As noted in our material & methods (page 15, line 547-548), SVs were defined as docked if there was no distance visible between the SV membrane and the active zone membrane. We have added the pixel size for clarification. Indeed, we do not observe an increase in release probability or first evoked response, which would correspond with an increased docked pool. However, we think that the increase in docked vesicles might contribute to an enhanced SV recruitment (see discussion).

> *(5) Figure 3: Vesicle cycling was monitored in only a limited condition. It is known that there are multiple pathways of vesicle cycling. Ideally, these pathways should be dissected. At least, the authors mention the possibility that they have missed some "positive" conditions.*

We fully agree with the reviewer's comment that vesicle recycling is complex with several parallel pathways involved. While we did not study individual endocytosis pathways, we used different assays covering various recycling pathways. The SypHy assay (Fig. 3c & f) combined with the 100 AP stimulation paradigm at room temperature predominantly addresses clathrin-mediated endocytosis. Additionally, the FM-64 dye assay at 37 degrees Celsius covers ultrafast endocytosis pathways as well as bulk endocytosis routes. Since

neither assay showed major effects, we decided not to pursue further experiments focusing on different endocytosis pathways.

> ***Reviewer #3 (Recommendations For The Authors):***
>
> *Major points:*
>
> *(1) Since all of the work here is culture-focussed, the in vivo phenotype is not as relevant, however the in vitro properties are. The incomplete Cre-dependent removal of SNX4 is concerning (especially axonal SNX4 levels identified via immunofluorescence), however, the main concern is that there was no profiling of the other molecular changes within these cultures. This is important, since there may be considerable alterations in the expression of a number of presynaptic proteins which may explain the observed phenotypes. Ideally, these cultures could have been profiled in an unbiased manner via mass spectrometry to identify potential changes in the presynaptic proteome, or at the very least the levels of key fusion molecules would have been assessed via Western blotting.*

We thank the reviewer for their suggestion and agree that mass spectrometry would strengthen the interpretation of the observed phenotype. However, due to contractual constraints, we are unable to pursue a mass spectrometry follow-up experiment. We agree that characterizing key fusion molecules is of potential interest. Therefore, based on literature, we selected a likely candidate, VAMP2, which did not show any alterations in expression levels when knocking out SNX4. Given the previously described role of SNX4 in the degradation pathway, one would expect increased degradation of key fusion molecules if they are recycled by SNX4. Other literature indicates that reduced levels of key fusion molecules, such as synaptotagmin or SNAP-25 (Broadie et al., 1994; Washbourne et al., 2001) , do not mimic our phenotype.

> *(2) The experiments reported in Figure 2, in particular those in 2c and 2d, suggest that overexpression of SNX4 has a dominant-negative effect on neurotransmitter release. This is strongly supported by the supplementary data during a stimulus train (particularly the start point of the 5 Hz train in Supplementary Figure 2). Therefore, the perceived rescue of EPSC charge in Figure 2f, 2g may be a result of SNX4 inhibiting neurotransmitter release. A determination of the impact of SNX4 overexpression (and level of overexpression) in WT neurons is essential to show that this is a bonefide rescue, rather than a direct inhibition by SNX4 overexpression.*

We thank the reviewer for their suggestion and agree that an additional experimental group (control + SNX4) would strengthen interpretation of the observed phenotype. We have now added a new experiment with an extra experimental condition with overexpression of SNX4 on a control background (Supplementary Fig. 3 page 21). This data shows that the amplitude and charge of the first evoked response were not affected in control + SNX4 neurons compared to control, and no differences were detected in the response to the 40 Hz stimulation train (Supplementary Fig. 3a-e). Together, these data suggest that SNX4 overexpression in itself does not affect the neurotransmission protocols studied in SNX4 cKO experiments.

> *(3) The experiments in Figure 3 clearly reveal a lack of effect of SNX4 depletion on synaptic vesicle endocytosis. However, the assumption that synaptic vesicle recycling is unaffected is a* little premature*. The fact that the second evoked SypHy peak is significantly larger than the first (Figures 3c-e) suggests that more vesicles may be recycling in KO neurons. Furthermore, the FM dye experiments do not aid interpretation, since there may be insufficient time (10 min) for new vesicles to be generated from endosomal intermediates experiments. Therefore, to confirm an absence of effect on*

> *recycling, the authors could either 1) perform the same experiment as 3c, but with 4 stimulation trains (to drive the system harder to reveal any phenotype) or 2) repeat the FM dye experiment but increase the time between loading and unloading to 30 min.*

We fully agree with the reviewers' comment that vesicle recycling is an important component to consider and is complex with several parallel pathways involved. We conducted multiple independent experiments covering the most significant recycling pathways. The SypHy assay (Fig. 3c & f) combined with the 100 AP stimulation paradigm at room temperature predominantly addresses clathrin-mediated endocytosis. Additionally, the FM-64 dye assay at 37 degrees Celsius covers ultrafast endocytosis pathways as well as bulk endocytosis routes. To further challenge the system and reveal recycling phenotypes, we included a second 100 AP stimulation in our SypHy assay. While only the increase of the second SypHy peak is significant, the absolute numbers do not differ much from the first peak (0,17 for control and 0,21 for KO second peak and 0,19 for control and 0,22 for KO first peak, Supplementary table1). We nevertheless do not see any effects on recycling after the second peak (mean decay time is 27 for control and 26 for KO Supplementary Table 1). A single 100 AP 40 Hz train depletes all the synchronous release (not shown) and most of the evoked charge (see Fig 2f), hence two of these trains with one minute recovery is already a very demanding protocol. Although increasing the time between loading and unloading to 30 minutes might uncover other recycling components, it has been shown that ultrafast endocytosis occurs within 30 seconds (Watanabe et al., 2013), suggesting that 10 minutes should provide enough time for synaptic vesicle recycling. This is also evident from the fact that we can significantly destain synapses loaded with FM dye by electrical stimulation (Fig 3j), indicating that synaptic vesicle recycling took place. Since neither assay showed major effects, we concluded that under these circumstances, synaptic recycling is not significantly affected. However, we cannot exclude the possibility that recycling deficits in SNX4 cKO neurons could be detected in other paradigms,

> *(4) There is no obvious effect on VAMP2 levels or location in SNX4 KO neurons (Figure 4). However, when one considers that SNX4 is proposed to have a role in VAMP2 trafficking, it is surprising that an experiment examining the live trafficking of VAMP2-SypHy was not performed. This would have revealed activity-dependent alterations that would have been missed by simply measuring VAMP2 expression and localization, and potentially provided a molecular explanation for the enhanced neurotransmitter release during a stimulus train.*

We appreciate the reviewer’s suggestion and agree that it could be a valuable experiment However, overexpressing a VAMP2-pHluorin construct might obscure potential phenotypes related to VAMP2 trafficking. SNX4 is expected to be involved in VAMP2 recycling, even with activity-dependent changes. Mis-sorted VAMP2 would accumulate in acidic vesicles, which could be masked by the VAMP2-pHluorin construct. Similarly, mis-sorting of other SNX4 cargo, such as the transferrin receptor, has been identified through lysosomal degradation, as shown by Western blot analysis of expression levels of the endogenous protein. We did not detect any differences in endogenous levels of VAMP2 within 21 days of SNX4 deletion (Fig 4), indicating that SNX4-dependent endosome sorting is not essential for VAMP2 recycling.

> *(5) The morphological data in Figure 5 report a series of small changes in docked vesicles and active zone length. In many cases, significance is obtained due to synapses being used as the experimental n, and thus inflating the statistical power. When one considers that no significant effect was observed on evoked release (apart from during a stimulus train), it suggests that the number of docked vesicles does not alter release probability in this system (which the authors point out). Instead, they suggest that an increased supply of vesicles is responsible, via increased recruitment to RRP/releasable pool (but not via increased recycling). If this is the case, it should have been reflected as an increase in the*

> *evoked SypHy response in Fig 2c,d (which is borderline significant). What may help is to determine the morphological landscape immediately after a stimulus strain, since this is the only condition where enhanced release is observed, and thus provide a morphological correlate to the physiological data.*

We fully agree with the reviewer's suggestion that an ultrastructural characterization immediately after a stimulus train would be informative. Unfortunately, contract constraints prevent us from performing this experiment. For our ultrastructural morphological data, we treated synapses as individual experimental *n* since it is not possible to determine whether synapses in a micronetwork on one sapphire originate from the same neuron. We used 18 independent sapphires from 3 independent pups to ensure the technical and biological replication of our data and measuring independent neurons. We fully agree with the reviewers comment to be careful with 'inflating the statistical power' due to potential nesting effects when using synapses as experimental n. To mitigate the potential nesting effect of analyzing multiple synapses per neuron, the intracluster correlation (ICC) is calculated per variable and per nesting effect. If ICC was close to 0.1, indicating that a considerable portion of the total variance can be attributed to e.g. synapse or sapphire, multilevel analysis was performed to accommodate nested data (Aarts et al., 2014).

> *Minor points*
>
> *(1) When a new mouse model is generated, it is usually accompanied by a thorough characterization of its properties. However, in this case, there was no information provided about the conditional SNX4 knockout mouse. This is surprising and at a minimum, the following should be provided a) the background strain, b) method of generation, c) the number of animals used to establish the colony, d) breeding strategy, e) backcrossing strategy, f) genotyping protocol.*

We apologize that a thorough characterization of our novel mouse model was lacking and therefore added this to our material & methods section (page 11, line 377-391).

> *(2) There is a noticeable difference between WT and KO neurons during train stimulation in Figure 2f, however, this appears to be due to the fact that there is a far higher EPSC charge to begin with in KO neurons. Why is there such a disparity when there is no difference in response to single pulses (Figures 2b-d) or presynaptic plasticity (Figure 2e)?*

We understand the reviewer's concern. We excluded an outlier (3x SD) in the KO dataset that drove the initial far higher EPSC charge in the graph (was already excluded for the statistics, Supplementary table 1). The average charge of the first pulse of 40Hz train is 41 pC and for KO neurons 58 pC, which did not differ significantly. These trains of Fig. 2f were recorded after 2 or 3 other stimulation paradigms, which can have affected the total charge released in the 40Hz train. That said, the proportional difference between groups is high comparable between Fig 2b-d and 2f, with a 37% increased average charge released in SNX4 cKO compared to control in the naïve response (Fig. 2d) and 41% increased response in the first response of the 40 Hz train (Fig. 2f), and rescued cells show a 53% reduction in average released charge compared to control in the naïve response compared to a 44% reduction in the first response of the 40 Hz train. Although the absolute values differ between these readouts, we conclude that the biological comparison between groups is consistent.

> *(3) Line 343-344 - "(Supplementary Figure 1a)" should be "(Figure 1a)".*

We thank the reviewer for this comment and adjusted this in the manuscript.

https://doi.org/10.7554/eLife.97910.2.sa0